國立臺灣大學電機資訊學院電信工程學研究所

碩士論文

Graduate Institute of Communication Engineering

College of Electrical Engineering and Computer Science

National Taiwan University

Master Thesis

在恆定模量限制下應用於低軌衛星通訊的寬主瓣波束成型技術

Beampattern Synthesis considering Constant Modulus Constraint for LEO Satellite Communication with Broadened Beam Service Areas

吳昱頡

Yu-Chieh Wu

指導教授: 蘇柏青 博士

Advisor: Borching Su, Ph.D.

中華民國 112 年 8 月

August, 2023

doi:10.6342/NTU202303344

Acknowledgements

首先我想謝謝蘇柏青老師這段時間的指導與教誨，老師提供許多在實務設計面上的意見與方向，並訓練我邏輯思考的能力，我才能在不斷跟老師的討論中漸漸勾勒出這篇論文的雛形。

接著我必須感謝實驗室的學長–林威廷參與這篇論文的研究和討論，另外，在寫論文時，謝謝你幫我修改文句並抓出語意盲點，每次的對談中你總是散發正面能量，讓我能夠懷抱希望去面對研究上的各種困難，寫論文的路上有你真的是一件很幸運的事！

謝謝丁文淵分享生活中發生的小故事或是 Stephen Boyd 的授課內容給我聽，讓我獲得許多有趣的新知，有時我們也會因為一個數學式討論到很晚，有結論時就會特別興奮，我想我會記得這些難忘的時刻。謝謝邱善晨幫我做紀錄讓我在報告後可以檢討，並在我有困難時伸出援手。謝謝實驗室的學弟妹們–張聿維、馬振洋、許曼楨在我每次報告時提出的意見，讓我的研究有進步的空間。

最後我要謝謝家人們的支持，讓我無後顧之憂地完成碩士學業，尤其謝謝女朋友林姿辰陪我度過這兩年研究生活，讓我不管在開心還是疲憊時都有人可以訴說並且獲得鼓勵。

doi:10.6342/NTU202303344

doi:10.6342/NTU202303344

摘要

衛星通訊在缺乏基礎通訊設施的偏遠地區因其仍能提供良好的網路連接而擁有優勢，然而因為衛星到地球的距離產生的路徑損耗，我們需要波束成型 (beamforming) 這個技術達成在特定方向上的接收地區有較高的訊號訊雜比 (SNR)，就我們所知，這篇論文提出第一個應用於衛星通訊的寬波束設計並使用考慮恆定模量限制的均勻矩形陣列波束成型器，目的是為了可以一次服務較大的地域範圍。在最佳化問題設計中，我們確保每一個在如此寬廣的服務地區內的使用者都可以接收到足夠高的訊雜比，因此獲得良好的衛星通訊品質，在衛星通訊中，為了確保每個服務地區接收到的訊號都能維持在某個強度以上，在波束圖形設計時需要考慮一個等通量模型。在本篇論文中，我們提出應用到不同情境時需考慮的兩個波束成型器設計，第一個設計目標是在恆定模量下壓抑不在服務範圍內的波束強度，在第二個情境中，波束將覆蓋所有和和衛星之間是直線連線的地球表面，並同樣地保持恆定模量，對於這兩個兩個不是凸函數最佳化的問題，我們使用半正定鬆弛技術和 Dattorro 的疊代演算法來解決，最後，模擬結果顯示我們可成功地在恆定模量下產生這兩個寬波束設計。

關鍵字：衛星通訊、低軌衛星、波束成型設計、恆定模量、等通量模型、均勻矩形陣列

doi:10.6342/NTU202303344

doi:10.6342/NTU202303344

Abstract

Satellite communication (SatComm) holds the advantage of providing Internet connectivity to rural and remote areas lacking communication infrastructures. Beamformer is significant in SatComm since it plays a crucial role in enhancing the transmission signal's direction and increasing the signal-to-noise ratio (SNR) in a specific direction. To our knowledge, the first Uniform Rectangular Array (URA) beamformer for SatCom which ensures PA efficiency that can serve large areas with beam-broadening approach is proposed. The optimization problem is designed to guarantee that user equipment (UEs) can experience sufficient SNR to establish communication link with the SAT transmitter within the SAT service areas. And the isoflux radiation mask guarantees that the transmitted signal maintains nearly equal strength within the SAT service areas, regardless of the SAT elevation angle. Two scenarios of beam-broadening optimization problems are formulated. In the first scenario, we aim to suppress the maximum signal power in out-of-beam SAT service areas with the required beamwidth under constant modulus constraint

doi:10.6342/NTU202303344

(CMC). In the second scenario, we aim to achieve Earth-coverage under CMC. Both of the non-convex problems are solved with semidefinite relaxation (SDR) and Dattorro iterative algorithm. The simulation results illustrate the URA beampattern with a broadened beamwidth, ensuring the minimum received SNR in SAT service areas. Additionally, the derived beamforming coefficients satisfy the CMC.

Keywords: Satellite communication (SatCom), low Earth orbit (LEO) satellite, beampattern synthesis, constant modulus constraint (CMC), isoflux radiation mask, Uniform Rectangular Array (URA)

doi:10.6342/NTU202303344

Contents

doi:10.6342/NTU202303344

doi:10.6342/NTU202303344

doi:10.6342/NTU202303344

doi:10.6342/NTU202303344

List of Figures

doi:10.6342/NTU202303344

doi:10.6342/NTU202303344

List of Tables

doi:10.6342/NTU202303344

doi:10.6342/NTU202303344

Chapter 1 Introduction

1.1 Introduction

Satellite communication (SatCom) has the advantage of providing Internet connectivity to remote areas and onboard aircraft or vessels, and it is anticipated to connect with a large number of user equipments (UEs) [12] [2] [19]. Beamforming, as one type of array processing technique, enhances the direction of the transmission signal, thus increasing the signal-to-noise ratio (SNR) in a specific direction. It is essential for SatCom because it helps overcome the great path loss resulting from the long distance between satellite (SAT) and Earth's surface [20] [15] [10] [12], which is much more severe than cellular communications.

A common beamforming approach is to adjust the phase of transmitted signal according to the array steering vector. If so, mainlobe beamwidth is inversely proportional to the antenna aperture [17]. Then SAT beam coverage becomes smaller as beamformer is assisted with more array elements. Although beam hopping technology can be applied for beam management, as the service areas per beam become smaller, beam scheduling comes to be more complex and frequent beam switching increases transition time delay [25] [22]. Therefore, to cover larger service areas, beam-broadening technique is important for achieving the required beamwidth.

doi:10.6342/NTU202303344

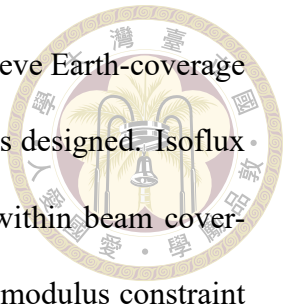

In [11] [24], LEO SAT beampattern synthesis which aims to achieve Earth-coverage was considered. Isoflux mask with mainbeam beamwidth of 100° was designed. Isoflux mask ensures that the transmitted signal has nearly equal strength within beam coverage area irrespective of the SAT elevation angle. However, constant modulus constraint (CMC) was not considered to ensure PA efficiency, and the designed beamformer may cannot apply in practical SATCOM.

To solve this problem, we referred to the problem formulations in [13] and [26] which considered beampattern synthesis with Dynamic Range Ratio (DRR) constraint and CMC respectively. We formulate a novel optimization problem that adopts beam-broadening approach under CMC constraint for SATCOM application. The Uniform Rectangular Array (URA) design problem is decomposed into two identical Uniform Linear Array (ULA) design problems [3][1][7], and the non-convex problem is solved with semidefinite relaxation (SDR) and Dattorro iterative algorithm [4]. In our knowledge, the first beamformer for SatCom which ensures PA efficiency that can serve large areas with beam-broadening is proposed.

doi:10.6342/NTU202303344

1.2 Contribution

In this thesis, we propose two beam-broadening approaches. The first beam-broadening approach aims to suppress the maximum signal power in out-of-beam SAT service areas with the required beamwidth under constant modulus constraint (CMC). The second beam-broadening approach aims to achieve Earth-coverage under CMC.

Furthermore, a novel isoflux mask applied for a URA transmitter is proposed to ensure the signal-to-noise ratio (SNR) within SAT service regions is larger than the requested minimum SNR.

doi:10.6342/NTU202303344

1.3 Notation

The notations used in this thesis are shown as follows. Boldfaced upper case letters represent matrices, boldfaced lower case letters represent column vectors, and italic letters represent scalar, e.g., $\mathbf{x}$, $\mathbf{X}$, and x. Superscripts $(\cdot)^*$, $(\cdot)^T$ and $(\cdot)^H$ denotes complex conjugate, transpose, Hermitian transpose respectively. The inner product of a and b is denoted as $\langle a, b \rangle$. The m-th row and n-th column entry of $\mathbf{X}$ are denoted as $[\mathbf{X}]_{m,n}$ .The complex $M \times N$ dimensional matrix and the complex $M \times 1$ dimensional vector are denoted by $\mathbb{C}^{M \times N}$ and $\mathbb{C}^M$. The set of integer and real number are denoted by $\mathbb{Z}$ and $\mathbb{R}$. Throughout this thesis we adopt zero-based indexing, e.g., $\mathbb{Z}_M = \{0, 1, ..., M-1\}$. $\mathbb{H}_+^M$ denotes the set of $M \times M$ positive semidefinite Hermitian matrix. $\mathbf{I}_M$ is a $M \times M$ identity matrix. $\Re\{\cdot\}$ denotes the real part and $\Im\{\cdot\}$ denotes the imaginary part of a complex number. We define $\mathrm{Tr}\{\cdot\}$ as the trace of a matrix. The expectation is denoted as $\mathbb{E}\{\cdot\}$. $\mathrm{vec}(\cdot)$ is to vectorize a matrix. $\otimes$ represents the Kronecker product. $\mathrm{rank}(\cdot)$ represents the rank of a matrix.

The rest of the thesis is organized as follows. In Chapter 2, we describe the system models for the URA and ULA systems. In Chapter 3, we formulate an URA optimization problem considering a controllable mainbeam beamwidth, the suppression of PSL, and the transmitter power constraints based on the real scenario of satellite communication. In Chapter 4, we reformulate the original URA problem into two ULA sub-problems. A semi-definite relaxation method is then applied to obtain the ULA weight coefficients. The set of URA weight coefficients is then composed from the resultant ULA weight coefficients. Simulation results are presented in Chapter 5 and conclusions are discussed in Chapter 6.

doi:10.6342/NTU202303344

Chapter 2 System Model

In this chapter, we will describe the system model of uniform rectangular array (URA) transmit beamformer that will be considered in our optimization problem. For convenience, we will introduce an uniform linear array (ULA) transmit beamformer first in section 2.1 where the transmitted signal of expression is derived. Then in section 2.2, we describe the system model of uniform rectangular array (URA) transmit beamformer.

2.1 Uniform linear array (ULA) transmit beamformer system model

In this section, the ULA transmit beamformer model is first shown. Then we derive the transmitted signal and the received signal of far-field receiver. In the premise that the transmitted signals are narrowband, the ULA transmit beampattern can be defined.

$s[n]$ is the transmitted data. In this thesis, the constant amplitude of $s[n]$ is hoped. The beamforming coefficients vector that we would like to design is denoted as $\mathbf{x}$, where $\mathbf{x} = [x_0\ x_1\ ...\ x_{M-1}]^T$. Discrete-time-to-continuous-time converters (D/C) with sampling rate f_s would turn digital signals into analog ones whose sampling interval is $T_s = \frac{1}{f_s}$. The pulse-shaping filter at transmitter, represented by $p_1(t)$ is then applied. The baseband

doi:10.6342/NTU202303344

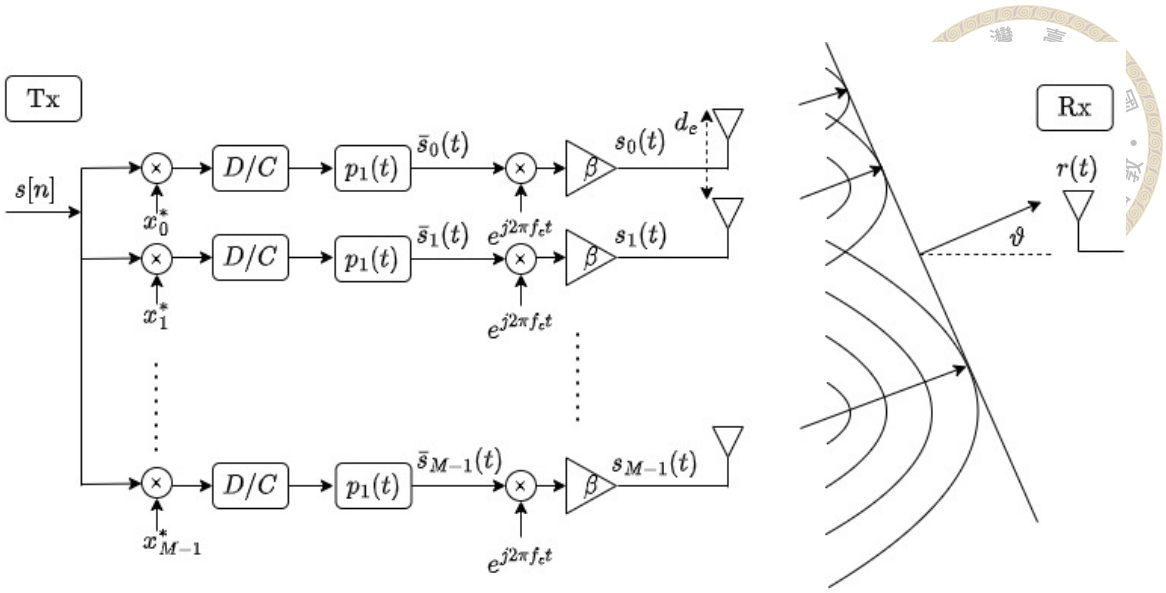

Figure 2.1: ULA transmit beamformer

signals $\bar{s}_0(t)$, $\bar{s}_1(t)$,..., $\bar{s}_{M-1}(t)$ are obtained

$$\bar{s}_m(t) = \sum_{n=-\infty}^{\infty} s[n] x_m^* p_1(t - nT_s), \quad m \in \mathbb{Z}_M \tag{2.1}$$

The baseband signals are transferred to Radio Frequency (RF) signal by up converters with carrier frequency f_c. Power amplifiers (PA) with gain β are considered to boost the transmitted signal voltage. Then, the transmitted signal at m-th antenna is shown as

$$s_m(t) = \beta \bar{s}_m(t) e^{j2\pi f_c t} \tag{2.2}$$

$$= \beta \sum_{n=-\infty}^{\infty} s[n] x_m^* p_1(t - nT_s) e^{j2\pi f_c t}, \quad m \in \mathbb{Z}_M. \tag{2.3}$$

We assume the transmitted signals are narrowband. The definition of narrowband applied in this thesis is based on fractional bandwidth.

Definition 2.1.1 (Fractional bandwidth)**.** Fractional bandwidth f_{FB} is defined as

$$f_{\text{FB}} = \frac{f_h - f_l}{f_h + f_l} \times 100\%, \tag{2.4}$$

where f_h and f_l are the highest and lowest components of the signal. The narrowband

doi:10.6342/NTU202303344

signal's f_{FB} is less than 1% and the wideband signal's f_{FB} is from 1% up to 25%.

Considering the ULA system model applied in Figure (2.1), the bandwidth of the transmitted RF signal f_{BW} is upper-bounded by the sampling rate f_s,i.e., $f_{\text{BW}} \leq f_s$. For convenience, we let $f_{\text{BW}} = f_s$. Then, if the transmitted signal is narrowband, we should ensure

$$f_{\text{FB}} = \frac{f_{\text{BW}}}{f_c} \times 100\% = \frac{f_s}{f_c} \times 100\% \leq 1\% \tag{2.5}$$

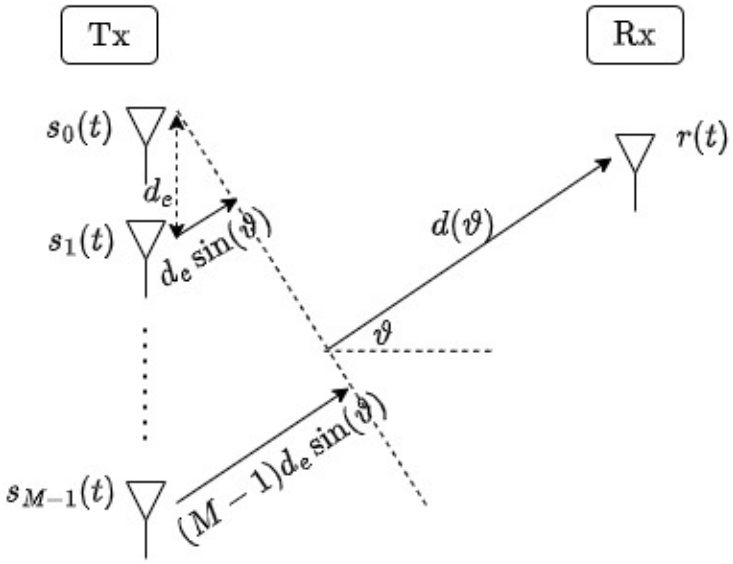

Figure 2.2: ULA channel model

To avoid the spatial aliasing for an ULA transmit beamformer with M sensors, the element spacing d_e should be smaller than $\frac{\lambda_{max}}{2}$, where λ_{max} is the wavelength corresponding to the maximum frequency component of transmitted signals. Since the transmitted signals are assumed narrowband, $\lambda_{max} = \lambda_c$ is selected, where λ_c is the wavelength corresponding to the carrier frequency. ϑ is the transmit antenna element radiation in the direction of departure (DOD) which is the angle between the transmitter's broadside and the direction toward the receiver, $\vartheta \in [-\frac{\pi}{2}, \frac{\pi}{2}]$.

doi:10.6342/NTU202303344

The channel model between the m-th transmit sensor and the receiver is represented by

$$h_m(t) = \delta(t - \frac{d(\vartheta)}{c} - \tau_m(\vartheta))), \tag{2.6}$$

where $d(\vartheta)$ is defined as the distance between the transmit array and the receiver. $\tau_m(\vartheta)$ is defined as the propagation delay between the m-th transmit antenna the 0-th transmit antenna, which is shown in figure 2.2.

$$\tau_m(\vartheta) = \frac{m d_e \sin(\vartheta)}{c} = \frac{m \sin(\vartheta)}{2 f_c}, \quad m \in \mathbb{Z}_M, \tag{2.7}$$

where c is the speed of light.

We assume the transmit and receive antenna element radiation are omni-directional, which are respectively represented by $D_{\text{T,e}}$ and $D_{\text{R,e}}$. If the receiver consists of $N_{a,R}$ antennas, the maximum receive antenna radiation is defined as

$$D_R = N_{a,R} \cdot D_{R,e} \tag{2.8}$$

doi:10.6342/NTU202303344

Then, the signal received by the receiver located in the far field can be expressed as

$$r(t) = \sum_{m=0}^{M-1} (s_m * h_m)(t) D_{T,e} D_R \tag{2.9}$$

$$= \sum_{m=0}^{M-1} s_m(t - \frac{d(\vartheta)}{c} - \tau_m(\vartheta)) D_{T,e} D_R \tag{2.10}$$

$$\downarrow s_m(t) = \beta \sum_{n=-\infty}^{\infty} s[n] x_m^* p_1(t - nT_s) e^{j2\pi f_c t} \tag{2.11}$$

$$= \sum_{m=0}^{M-1} \left[\beta \sum_{n=-\infty}^{\infty} s[n] x_m^* p_1(t - \frac{d(\vartheta)}{c} - \tau_m(\vartheta) - nT_s) e^{j2\pi f_c (t - \frac{d(\vartheta)}{c} - \tau_m(\vartheta))} \right] D_{T,e} D_R \tag{2.12}$$

$$\downarrow \tau_m(\vartheta) = \frac{m \sin(\vartheta)}{2 f_c} \text{ from (2.7)} \tag{2.13}$$

$$= \beta e^{j2\pi f_c (t - \frac{d(\vartheta)}{c})} D_{T,e} D_R \sum_{m=0}^{M-1} x_m^* e^{-j2\pi f_c \tau_m(\vartheta)} \sum_{n=-\infty}^{\infty} s[n] p_1(t - \frac{d(\vartheta)}{c} - T_s(\frac{m \sin(\vartheta) f_s}{2 f_c} + n)). \tag{2.14}$$

Since the transmitted signals are assumed narrowband, $\frac{f_s}{f_c} \ll 1$ according to (2.5),

$$p_1(t - \frac{d(\vartheta)}{c} - T_s(\frac{m \sin(\vartheta) f_s}{2 f_c} + n)) \approx p_1(t - \frac{d(\vartheta)}{c} - nT_s) \tag{2.15}$$

Then we can rewrite $r(t)$ as

$$r(t) = \beta e^{j2\pi f_c (t - \frac{d(\vartheta)}{c})} D_{T,e} D_R \sum_{m=0}^{M-1} x_m^* e^{-j2\pi f_c \tau_m(\theta)} \left[\sum_{n=-\infty}^{\infty} s[n] p_1(t - \frac{d(\vartheta)}{c} - nT_s) \right] \tag{2.16}$$

$$= \beta e^{j2\pi f_c (t - \frac{d(\vartheta)}{c})} D_{T,e} D_R \left[\sum_{n=-\infty}^{\infty} s[n] p_1(t - \frac{d(\vartheta)}{c} - nT_s) \right] \mathrm{B}(\mathbf{x}, \vartheta), \tag{2.17}$$

where $\mathrm{B}(\mathbf{x}, \vartheta)$ is defined as the ULA transmit beampattern.

doi:10.6342/NTU202303344

Definition 2.1.2 (ULA transmit beampattern)**.** The ULA transmit beampattern $\mathrm{B}(\mathbf{x}, \vartheta)$ is represented as

$$\mathrm{B}(\mathbf{x}, \vartheta) \triangleq \mathbf{x}^H \mathbf{a}(\vartheta) = \sum_{m=0}^{M-1} x_m^* e^{-j2\pi f_c \tau_m(\vartheta)}, \tag{2.18}$$

where $\mathbf{a}(\vartheta) = [1\ e^{-j2\pi f_c \tau_1(\vartheta)}\ \ldots\ e^{-j2\pi f_c \tau_{M-1}(\vartheta)}]^T$ is defined as the steering vector.

2.2 Uniform Rectangular Array (URA) transmit beamformer system model

In this section, we follow the assumption that the transmitted signal is narrowband to describe the system model for an URA transmit beamformer. Then we derive the transmitted signal and the received signal of far-field receiver. Lastly, the URA transmit beampattern is defined.

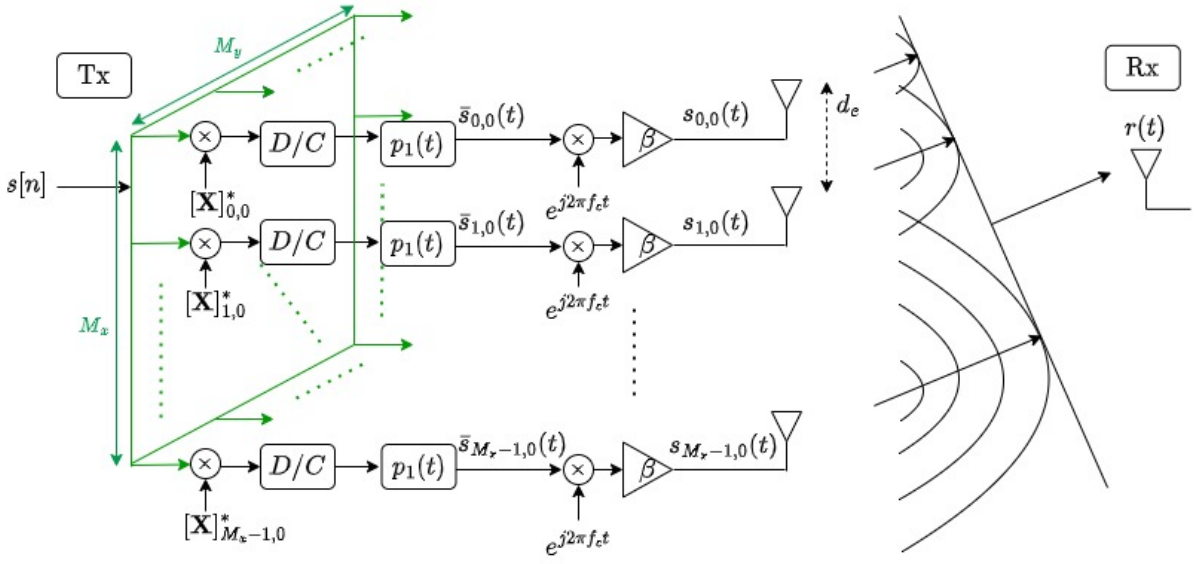

Figure 2.3: URA transmit beamformer

An URA is consisted with $M_x \times M_y$ sensors, where M_x is the number of sensors at the x-axis and M_y is the number of sensors at the y-axis. The beamforming coefficients are defined as $\mathbf{X} \in \mathbb{C}^{M_x \times M_y}$. The element spacing on the x-axis and y-axis is same to the

doi:10.6342/NTU202303344

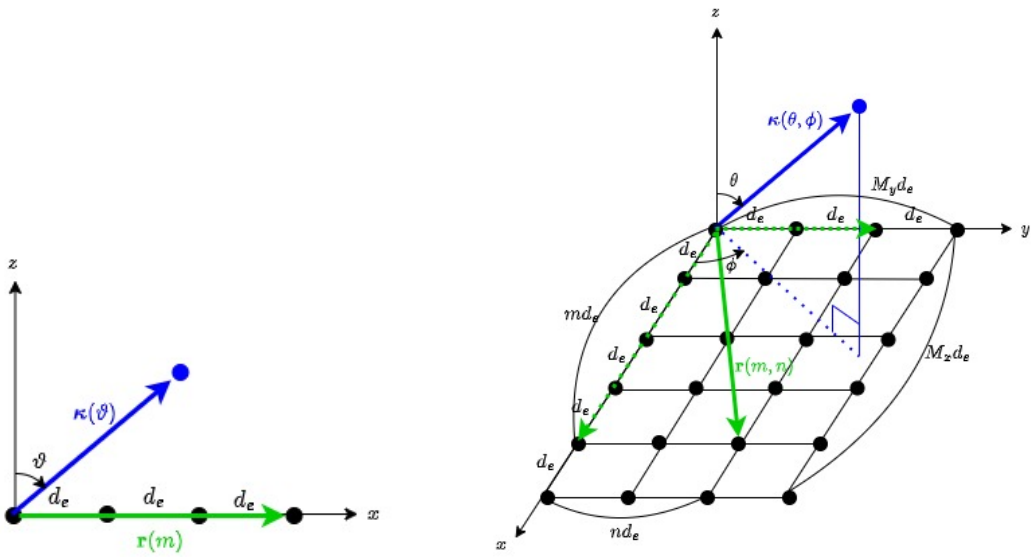

(a) ULA (b) URA

Figure 2.4: ULA and URA transmit beamformer geometry

ULA, d_e.

An ULA is a special case of an URA if either M_x or M_y reduces to one, which is shown in Fig 2.4(a). We first define $\boldsymbol{\kappa}(\vartheta)$ as the array look direction which is a unit vector from a ULA. The z-axis can be considered to be the direction perpendicular to the plane of the transmit array. In this way, ϑ is as same as that defined in figure 2.1. The $\mathbf{r}(m)$ is defined as the vector pointed to the m-th sensor from the 0-th sensor, e.g., in the case of ULA, $\mathbf{r}(m) = md_e$. Then, the time delay of the m-th sensor with respect to the 0-th sensor described in Fig 2.2 is equivalent to the inner product of $\mathbf{r}(m)$ and $\boldsymbol{\kappa}(\vartheta)$, e.g., $\langle \mathbf{r}(m), \boldsymbol{\kappa}(\vartheta) \rangle = md_e \times \cos(\frac{\pi}{2} - \vartheta) = md_e \sin(\vartheta)$. Thus, the propagation delay between the m-th transmit antenna and the 0-th transmit antenna can be expressed as (2.19).

$$\tau_m(\vartheta) = \frac{\langle \mathbf{r}(m), \boldsymbol{\kappa}(\vartheta) \rangle}{c} \tag{2.19}$$

doi:10.6342/NTU202303344

The beampattern of an ULA can be rewritten as (2.20).

$$\mathrm{B}(\mathbf{x}, \vartheta) = \sum_{m=0}^{M-1} x_m^* e^{-j2\pi f_c(\frac{\langle \mathbf{r}(m), \boldsymbol{\kappa}(\vartheta) \rangle}{c})}, \tag{2.20}$$

Compared with Fig 2.4(a) and 2.4(b), we could extend $\boldsymbol{\kappa}(\vartheta)$ into $\boldsymbol{\kappa}(\theta, \phi)$ and extend $\mathbf{r}(m)$ into $\mathbf{r}(m, n)$ for a planar array. Note that θ here is defined as the angle between the z-axis and the transmitted signal direction toward the receiver, where $\theta \in [0, \frac{\pi}{2}]$, and ϕ is defined as the azimuth angle of the projection of $\boldsymbol{\kappa}(\theta, \phi)$ on the xy plane, where $\phi \in [0, 2\pi]$. Then, the inner product of $\mathbf{r}(m, n)$ and $\boldsymbol{\kappa}(\theta, \phi)$ is obtained. The projection of $\boldsymbol{\kappa}(\theta, \phi)$ on the xy-plane is $\sin(\theta)$. Thus, the projection of $\boldsymbol{\kappa}(\theta, \phi)$ on the x-axis and on the y-axis can be derived as $\cos(\phi)\sin(\theta)$ and $\sin(\phi)\sin(\theta)$, respectively. The inner product of $\mathbf{r}(m, n)$ and $\boldsymbol{\kappa}(\theta, \phi)$ is equivalent to $\begin{bmatrix} md_e & nd_e \end{bmatrix} \begin{bmatrix} \cos(\phi)\sin(\theta) \\ \sin(\phi)\sin(\theta) \end{bmatrix}$.

With this transformation, we can obtain the inter-antenna delay between the (m, n)-th antenna and the $(0, 0)$-th antenna of an URA transmit beamformer. Similar to (2.19),

$$\tau_{m,n}(\theta, \phi) = \frac{\langle \mathbf{r}(m, n), \boldsymbol{\kappa}(\theta, \phi) \rangle}{c} \tag{2.21}$$

$$= \frac{md_e \sin(\theta)\cos(\phi) + nd_e \sin(\theta)\sin(\phi)}{c}, \tag{2.22}$$

Similar to the ULA transmit beampattern defined in (2.20), the beampattern of an URA can be defined as well.

Definition 2.2.1 (URA transmit beampattern)**.** The URA transmit beampattern $\tilde{\mathrm{B}}(\mathbf{X}, \theta, \phi)$ is defined as

$$\tilde{\mathrm{B}}(\mathbf{X}, \theta, \phi) = \sum_{m=0}^{M_x-1} \sum_{n=0}^{M_y-1} [\mathbf{X}]_{m,n}^* e^{-j2\pi f_c \tau_{m,n}(\theta,\phi)} \tag{2.23}$$

doi:10.6342/NTU202303344

Under the assumption that the transmitted signals are narrowband, we first recall the received signal $r(t)$ whose transmitter is an ULA with the transmission angle ϑ, described in (2.17),

$$r(t) = \beta e^{j2\pi f_c(t-\frac{d(\vartheta)}{c})} D_{T,e} D_R \left[\sum_{n=-\infty}^{\infty} s[n] p_1(t - \frac{d(\vartheta)}{c} - nT_s) \right] \mathrm{B}(\mathbf{x}, \vartheta) \tag{2.24}$$

For the system model with an URA transmit beamformer, we define $d(\theta, \phi)$ as the distance between the transmitter and a receiver at far field with the elevation angle θ and the azimuth angle ϕ. After substituting $d(\vartheta)$ in (2.24) with $d(\theta, \phi)$ and substituting $\mathrm{B}(\mathbf{x}, \theta)$ with $\tilde{\mathrm{B}}(\mathbf{X}, \theta, \phi)$, we can obtain the received signal at the far field as follows.

$$r(t) = \beta e^{j2\pi f_c(t-\frac{d(\theta,\phi)}{c})} D_{T,e} D_R \left[\sum_{n=-\infty}^{\infty} s[n] p_1(t - \frac{d(\theta, \phi)}{c} - nT_s) \right] \tilde{\mathrm{B}}(\mathbf{X}, \theta, \phi) \tag{2.25}$$

doi:10.6342/NTU202303344

doi:10.6342/NTU202303344

Chapter 3 Problem Formulation

In this chapter, we take the real implementation of SatComm into account and formulate an optimization problem for desinging the URA transmit beamformer. In section 3.1, field of views of a satellite (SAT) is decided according to the calculation of effective illuminated region of SAT. The link budget between the satellite and the UE is then derived in section 3.2. The loss during the transmission is detailedly considered. Among them, free-space propagation loss is dominant and an isoflux mask on angular domain is formulated. Furthermore, the signal-to-noise ratio (SNR) can be calculated. In section 3.3, to obtain a high enough channel capacity, the lower bound of mainlobe is derived according to link budget calculation. Lastly, we sum up the requirements and formulate an optimization problem.

doi:10.6342/NTU202303344

3.1 Field of view (FoV) of a satellite

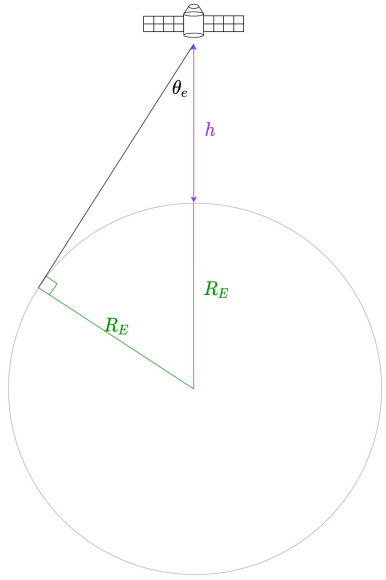

Figure 3.1: Scenario of SAT FoV

In this section, the derivation of SAT Field of view (FoV) is shown first. Suppose the boresight of the satellite points vertically towards the ground. h denotes the vertical distance between the satellite and the Earth, which also represents the minimum distance between the satellite and the ground. Then, we define the angle between h and the Earth's tangent point as θ_e, $\theta_e \in [0, \frac{\pi}{2}]$. This angle is also related with the radius of earth R_E.

$$\sin(\theta_e) = \frac{R_E}{h + R_E} \tag{3.1}$$

$$\Rightarrow \theta_e = \sin^{-1}(\frac{R_E}{h + R_E}) \tag{3.2}$$

Signals transmitted in the direction $\theta \in [\theta_e, \frac{\pi}{2}]$ would not reach the Earth due to the Earth's curvature, so we only need to consider the $\theta \in [0, \theta_e]$ in the beampattern design. Consequently, the field of view (FoV) of a SAT is defined as $2\theta_e$.

doi:10.6342/NTU202303344

3.2 Link budget analysis for SAT downlink

In this section, we analyze the link budget for the SAT downlink connection. First, we derive the transmission power towards a particular direction, then consider path loss along the downlink propagation, and finally calculate the received power and its corresponding signal-to-noise ratio (SNR). To ensure the SAT coverage area enjoys enough channel capacity, the derivation of link budget enables us to evaluate the required lower bound of beampattern within the SAT service areas.

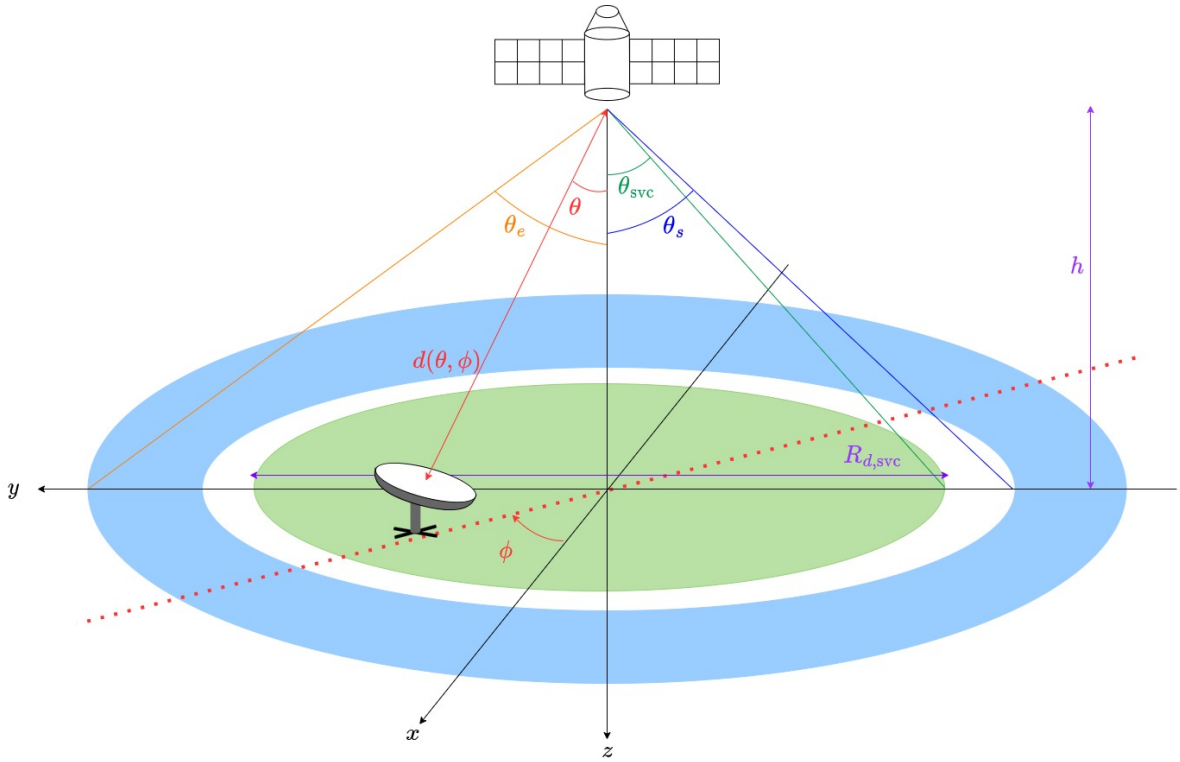

Figure 3.2: SAT beam service areas illustration

SAT spot beam coverage area is associated with the SAT service angle θ_{svc} and the SAT altitude h, where we define the SAT service angle θ_{svc} as the angle with respect to the antenna boresight at which the mainbeam pattern covers. The SAT service beamwidth is corresponding to $2\theta_{\text{svc}}$. We define the slant angle between the SAT transmitter's boresight and the UE's antenna as θ. ϕ is the azimuth angle between the x-axis of the satellite and

doi:10.6342/NTU202303344

the receiver. The mainlobe of URA transmit beampattern is defined $\forall\theta \in [0, \theta_{\text{svc}}]$ and the sidelobe of beampattern is defined $\forall\theta \in [\theta_s, \theta_e]$. The angle set between θ_{svc} and θ_s is called the transition region which is the buffer region between mainlobe and sidelobe. Note that θ_{svc}, θ, θ_s are all defined in $[0, \frac{\pi}{2}]$.

3.2.1 Signal-to-noise ratio (SNR) analysis

In this section, signal-to-noise ratio (SNR) analysis is derived through the calculation of transmitted signal power, transmission loss and thermal noise power. First, recall the system of the URA transmit beamformer from (2.3) and recall the received signal $r(t)$ from (2.25) under the assumption that the transmitted signals are narrowband.

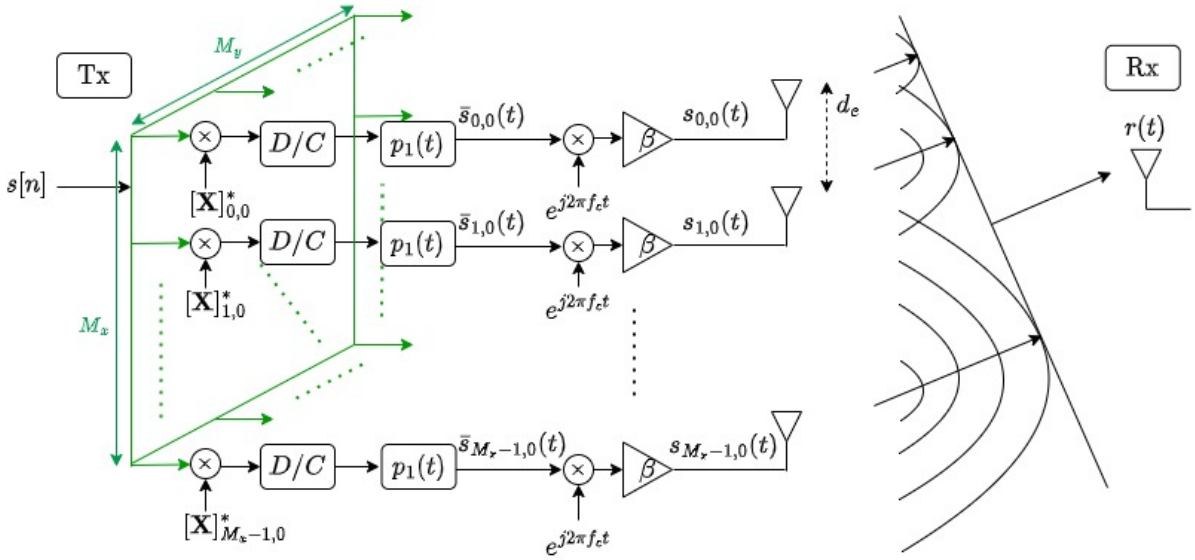

Figure 3.3: URA transmit beamformer

$$r(t) = \beta e^{j2\pi f_c(t-\frac{d(\theta,\phi)}{c})} D_{T,e} D_R \left[\sum_{n=-\infty}^{\infty} s[n] p_1(t - \frac{d(\theta,\phi)}{c} - nT_s)\right] \tilde{\mathbf{B}}(\mathbf{X}, \theta, \phi)$$

With receive pulse shaping filter, we assume the receiver is able to recover $s[k]$ from received signal $r(t)$ at sample time $t = kT_s$, the power of the sampled data at receiver $y[k]$

doi:10.6342/NTU202303344

becomes

$$\mathbb{E}\{|y[k]]|^2\} = \beta^2 \mathbb{E}\{|s[k]|^2\} G_{T,e} G_R |\tilde{\mathbf{B}}(\mathbf{X}, \theta, \phi)|^2, \tag{3.3}$$

where $G_{T,e} = |D_{T,e}|^2$ and $G_R = |D_R|^2$.

We define P_T as the transmitted signal power. Ω_T is the equivalent resistance of the transmitter. Generally, we let it be 1.

$$P_T = \frac{\beta^2 \mathbb{E}\{|s[k]|^2\} \sum_{m=0}^{M_x-1} \sum_{n=0}^{M_y-1} |[\mathbf{X}]_{m,n}|^2}{\Omega_T} \quad \text{(watt)} \tag{3.4}$$

The transmit antenna array gain is denoted as $G_T(\mathbf{X}, \theta, \phi)$.

$$G_T(\mathbf{X}, \theta, \phi) = \frac{G_{T,e} |\tilde{\mathbf{B}}(\mathbf{X}, \theta, \phi)|^2}{\sum_{m=0}^{M_x-1} \sum_{n=0}^{M_y-1} |[\mathbf{X}]_{m,n}|^2} \tag{3.5}$$

For convenience, we let $G_{T,e} = 1$

$$G_T(\mathbf{X}, \theta, \phi) = \frac{|\tilde{\mathbf{B}}(\mathbf{X}, \theta, \phi)|^2}{\sum_{m=0}^{M_x-1} \sum_{n=0}^{M_y-1} |[\mathbf{X}]_{m,n}|^2} \tag{3.6}$$

Thus, the power of received signal is denoted as $P_R(\mathbf{X}, \theta, \phi)$

$$P_R(\mathbf{X}, \theta, \phi) = \mathbb{E}\{|y[k]|^2\} \tag{3.7}$$

$$= P_T G_T(\mathbf{X}, \theta, \phi) G_R. \tag{3.8}$$

However, as we known, we also have to consider the power loss during the transmission. We describe the transmission loss $L(\theta, \phi)$ as follows[21].

$$L(\theta, \phi) = L_{\text{c,T}} L_{\text{c,R}} L_{\text{fs}}(\theta, \phi) L_{\text{a}} L_{\text{sm}} L_{\text{sl}}, \tag{3.9}$$

where $L_{\text{c,T}}$ is cable loss in transmitter, $L_{\text{c,R}}$ is cable loss in receiver, $L_{\text{fs}}(\theta, \phi)$ is the free-

doi:10.6342/NTU202303344

space propagation loss, L_{a} is atmospheric path loss, L_{sm} is shadowing loss, and L_{sl} is scintillation loss.

Among them, free-space propagation loss is dominant. In this thesis, we adopt the free-space path loss (FSPL) formula derived from the Friis transmission formula[8]. We import angular information into this equation and reformulate it as:

$$L_{\text{fs}}(\theta,\phi) = \left(\frac{4\pi d(\theta,\phi)}{\lambda}\right)^2, \tag{3.10}$$

where $d(\theta,\phi)$ is the distance between SAT and the user equipment (UE), λ is the wavelength of the transmitted signal.

The distance between SAT and a UE is derived with the consideration of Earth curvature.

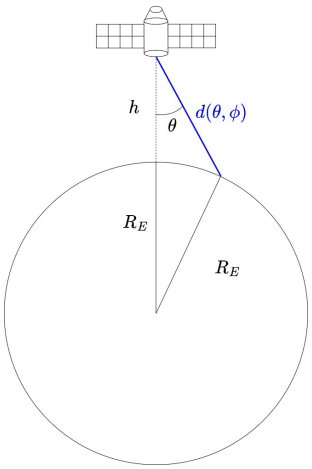

Figure 3.4: SAT-UE scenario

According to the cosine law,

$$R_E^2 = d^2(\theta,\phi) + (h+R_E)^2 - 2d(\theta,\phi)(h+R_E)\cos(\theta) \tag{3.11}$$

$$\Rightarrow 0 = d^2(\theta,\phi) + h^2 + 2hR_E - 2d(\theta,\phi)(h+R_E)\cos(\theta) \tag{3.12}$$

$$\Rightarrow 0 = d^2(\theta,\phi) - 2d(h+R_E)\cos(\theta) + (h^2+2hR_E) \tag{3.13}$$

doi:10.6342/NTU202303344

After solving equation (3.13), $d(\theta, \phi)$ can solved

$$d(\theta, \phi) = (h + R_E)\cos(\theta) - \sqrt{R_E^2 - (h + R_E)^2 \sin^2(\theta)}, \tag{3.14}$$

where h is the SAT altitude, and R_E represents the radius of the Earth. Combined (3.10) with (3.14), the free-space path loss could be rewritten as

$$L_{\text{fs}}(\theta, \phi) = \sigma^2(\theta) \left(\frac{4\pi h}{\lambda}\right)^2, \tag{3.15}$$

where $\sigma(\theta)$ is defined as the URA isoflux mask

$$\sigma(\theta) = \frac{\left[(h + R_E)\cos(\theta) - \sqrt{R_E^2 - (h + R_E)^2 \sin^2(\theta)}\right]}{h}. \tag{3.16}$$

After considering the transmission loss, the received signal power is adjusted as

$$P_R(\mathbf{X}, \theta, \phi) = \frac{P_T G_T(\mathbf{X}, \theta, \phi) G_R}{L(\theta, \phi)} \tag{3.17}$$

$$= \frac{P_T G_T(\mathbf{X}, \theta, \phi) G_R}{\sigma^2(\theta) L_0}, \tag{3.18}$$

$$\text{where} \quad L_0 = L_{\text{c,T}} L_{\text{c,R}} L_{\text{a}} L_{\text{sm}} L_{\text{sl}} \left(\frac{4\pi h}{\lambda}\right)^2. \tag{3.19}$$

We consider the thermal noise power at UEs. It can be formulated as

$$P_{\text{N}} = k T_{\text{sys}} f_{\text{BW}}, \tag{3.20}$$

where $k = 1.38 \times 10^{-23}$ [watt $\cdot$ sec/K] is the Boltzmann constant, f_{BW} [Hz] is the channel bandwidth, and T_{sys} [K] is the receiver system temperature:

$$T_{\text{sys}} = T_{\text{noise}} + T_{\text{a,R}}, \tag{3.21}$$

doi:10.6342/NTU202303344

$$T_{\text{noise}} = T_0(10^{\frac{N_f\,[dB]}{10}} - 1), \tag{3.22}$$

where $T_0 = 290$ [K] is the standard temperature, N_f [dB] is the noise figure of front-end circuits, and $T_{\text{a,R}}$ [K] is the received antenna temperature. Then we obtain

$$T_{\text{sys}}\,[K] = T_0\,[K](10^{\frac{N_f\,[dB]}{10}} - 1) + T_{\text{a,R}}\,[K]. \tag{3.23}$$

The signal-to-noise ratio is defined as

$$\text{SNR}(\mathbf{X}, \theta, \phi) = \frac{P_R(\mathbf{X}, \theta, \phi)}{P_N} \tag{3.24}$$

$$= \frac{P_T G_T(\mathbf{X}, \theta, \phi) G_R}{\sigma^2(\theta) P_N L_0}, \tag{3.25}$$

$$= \frac{P_T G_T(\mathbf{X}, \theta, \phi) G_R}{\sigma^2(\theta) k T_{\text{sys}} f_{\text{BW}} L_0}, \tag{3.26}$$

where $G_T(\mathbf{X}, \theta, \phi) = \dfrac{|\tilde{\mathbf{B}}(\mathbf{X}, \theta, \phi)|^2}{\sum_{m=0}^{M_x-1} \sum_{n=0}^{M_y-1} |[\mathbf{X}]_{m,n}|^2}$ is shown in (3.6).

doi:10.6342/NTU202303344

3.3 Problem formulation

In this section, we formulate the problem of interest. We first calculate the mainlobe lower bound in Section 3.3.1 in order to ensure the signal quality within the SAT service areas. We will consider the peak sidelobe level (PSL) suppression in Section 3.3.2 to connect to our objective of suppressing out-of-beam signal power. In Section 3.3.3, we introduce two kinds of weight coefficients constraints, i.e., constant modulus constraint (CMC) and dynamic range ratio (DRR) constraint. Eventually, two scenarios of beam-broadening optimization problems are formulated. In the first scenario, we aim to suppress the maximum signal power in out-of-beam SAT service areas with the required beamwidth under constant modulus constraint (CMC). In the second scenario, we aim to achieve Earth-coverage under CMC.

3.3.1 Mainlobe lower bound calculation

In the SAT beam service areas, we would like to ensure UEs enjoy the channel capacity larger than C_{min}.

$$C(\mathbf{X},\theta,\phi) = f_{\text{BW}}\log_2(1+\text{SNR}(\mathbf{X},\theta,\phi) \geq f_{\text{BW}}\log_2(1+\text{SNR}_{\text{min}}) = C_{\text{min}}. \tag{3.27}$$

We aim to derive the beampattern mainlobe lower bound to ensure the UEs in the mainlobe coverage all receive the SNRs higher than SNR_{min}. Recall the received SNR (3.26),

$$\text{SNR}(\mathbf{X},\theta,\phi) = \frac{P_T G_T(\mathbf{X},\theta,\phi) G_R}{\sigma^2(\theta) k T_{\text{sys}} f_{\text{BW}} L_0} \tag{3.28}$$

$$= \frac{\beta^2 \mathbb{E}\{|s[k]|^2\}|\tilde{\mathbf{B}}(\mathbf{X},\theta,\phi)|^2 G_R}{\sigma^2(\theta) k T_{\text{sys}} f_{\text{BW}} L_0} \tag{3.29}$$

doi:10.6342/NTU202303344

We assume $\beta^2 \cdot \mathbb{E}\{|s[k]|^2\} = 1$, the SNR turns into

$$\text{SNR}(\mathbf{X}, \theta, \phi) = \frac{|\tilde{\text{B}}(\mathbf{X}, \theta, \phi)|^2 G_R}{\sigma^2(\theta) k T_{\text{sys}} f_{\text{BW}} L_0} \tag{3.30}$$

Then, the following inequality should hold.

$$\frac{|\tilde{\text{B}}(\mathbf{X}, \theta, \phi)|^2 G_R}{\sigma^2(\theta) k T_{\text{sys}} f_{\text{BW}} L_0} \geq \text{SNR}_{\text{min}}, \quad \forall \theta \in [0, \theta_{\text{svc}}], \ \forall \phi \in [0, 2\pi] \tag{3.31}$$

$$\Rightarrow |\tilde{\text{B}}(\mathbf{X}, \theta, \phi)|^2 \geq \frac{\text{SNR}_{\text{min}} k T_{\text{sys}} f_{\text{BW}} L_0 \sigma^2(\theta)}{G_R} \tag{3.32}$$

$$\Rightarrow |\tilde{\text{B}}(\mathbf{X}, \theta, \phi)| \geq \alpha \sigma(\theta) \tag{3.33}$$

We define α as

$$\alpha = \sqrt{\frac{\text{SNR}_{\text{min}} k T_{\text{sys}} f_{\text{BW}} L_0}{G_R}}. \tag{3.34}$$

3.3.2 Peak sidelobe level (PSL) suppression

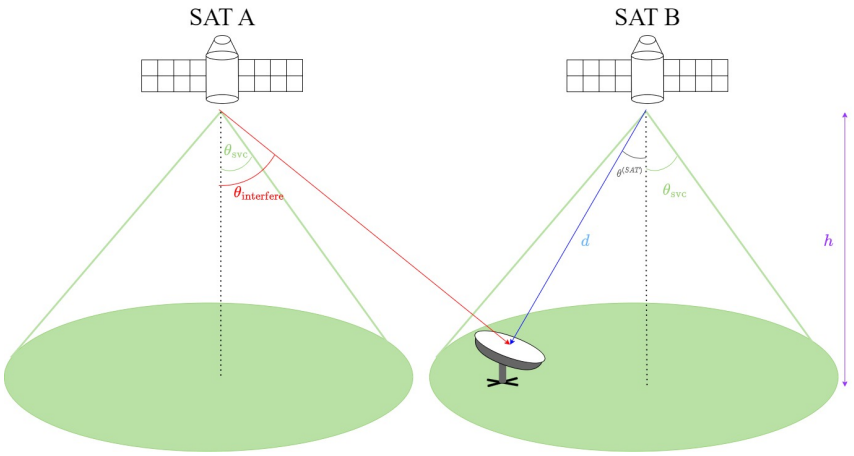

Figure 3.5: SAT out-of-beam interference illustration

We define the sidelobe of a satellite as $\theta \in [\theta_s, \theta_e]$, where θ_e is the half of the FoV of a satellite and θ_s is the angle shown in figure 3.2. If the mainlobe of a satellite is overlapped with the sidelobe of another satellite whose sidelobe power is significant, the communication quality in this area may decrease severely because of the strong interference. For

doi:10.6342/NTU202303344

example, the UE in figure 3.5 may be interfered by the power leakage from SAT A if the signal power at angle $\theta_{\text{interfere}} \in [\theta_s, \theta_e]$ is large. Therefore, to avoid the power leakage to the sidelobe regions, we should suppress the maximum power of received signal, $\max\{P_R(\mathbf{X}, \theta, \phi)\}$, for all $\theta \in [\theta_s, \theta_e]$. Note that $P_R(\mathbf{X}, \theta, \phi)$ has been defined in (3.17).

$$P_R(\mathbf{X}, \theta, \phi) = \frac{P_T G_T(\mathbf{X}, \theta, \phi) G_R}{\sigma^2(\theta) L_0} \tag{3.35}$$

$$= \frac{\beta^2 \mathbb{E}\{|s[k]|^2\} |\tilde{\mathbf{B}}(\mathbf{X}, \theta, \phi)|^2 G_R}{\sigma^2(\theta) L_0} \tag{3.36}$$

Then, follow the assumption $\beta^2 \cdot \mathbb{E}\{|s[k]|^2\} = 1$, $P_R(\mathbf{X}, \theta, \phi)$ is rewritten as

$$P_R(\mathbf{X}, \theta, \phi) = \frac{|\tilde{\mathbf{B}}(\mathbf{X}, \theta, \phi)|^2 G_R}{\sigma^2(\theta) L_0} \tag{3.37}$$

Since G_R and L_0 are constant, minimizing the peak sidelobe power equals to

$$\underset{\mathbf{X} \in \mathbb{C}^{M_x \times M_y}}{\text{minimize}} \quad \sup_{\theta \in [\theta_s, \theta_e], \phi \in [0, 2\pi]} \frac{|\tilde{\mathbf{B}}(\mathbf{X}, \theta, \phi)|}{\sigma(\theta)} \tag{3.38}$$

doi:10.6342/NTU202303344

3.3.3 Constant modulus constraint (CMC) and dynamic range ratio (DRR) constraint

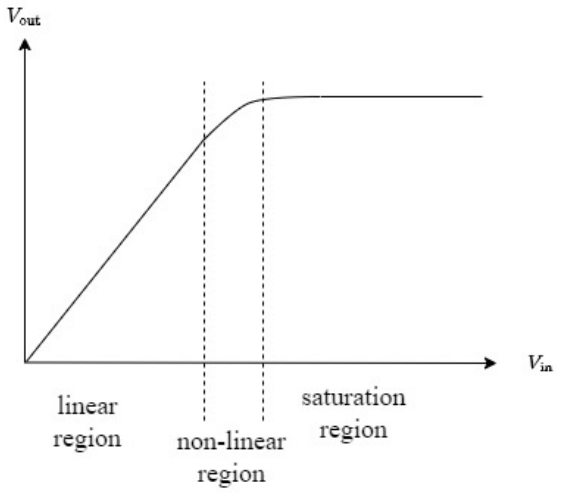

Figure 3.6: Relation between V_{in} and V_{out} of an amplifier [18]

Recall the system model of an URA described in figure 2.3, we can find that V_{in} of PA is the magnitude of $\bar{s}_{m,n}(t)e^{j2\pi f_c t}$. The exponential term wouldn't affect the magnitude. Since $\bar{s}_{m,n}(t) = \sum_{k=-\infty}^{\infty} s[k][\mathbf{X}]^*_{m,n} p_1(t - kT_s)$, we desire the maximum of $|\bar{s}_{m,n}(t)|$ for all $m \in \mathbb{Z}_{M_x}$ and $n \in \mathbb{Z}_{M_y}$ to be at the boundary between linear region and non-linear region. This ensures the satellite push the maximum power toward the UEs effectively, which leads to high SNR at receivers. Therefore, we want the beamforming coefficients to be constant modulus.

Definition 3.3.1 (Constant modulus constraint (CMC))**.** CMC is defined as

$$\max_{m,n}\{|[\mathbf{X}]_{m,n}|\} = \min_{m,n}\{|[\mathbf{X}]_{m,n}|\}, \quad m \in \mathbb{Z}_{M_x}, n \in \mathbb{Z}_{M_y}, \tag{3.39}$$

However, the constraint of constant modulus loses lots of degree of freedom. Therefore, we may concern dynamic range ratio (DRR) constraints instead of constant modulus

doi:10.6342/NTU202303344

constraints in some practical scenarios.

Definition 3.3.2 (Dynamic range ratio (DRR))**.** DRR is defined as

$$\mathrm{DRR}(\mathbf{X}) = \frac{\max\limits_{m,n}\{|[\mathbf{X}]_{m,n}|\}}{\min\limits_{m,n}\{|[\mathbf{X}]_{m,n}|\}}, \quad m \in \mathbb{Z}_{M_x}, n \in \mathbb{Z}_{M_y}, \tag{3.40}$$

Let $\zeta = \mathrm{DRR}(\mathbf{X})$, and $\mu = \min\limits_{m,n}\{|[\mathbf{X}]_{m,n}|\}$. We obtain

$$\mu \le |[\mathbf{X}]_{m,n}| \le \mu\zeta, \quad m \in \mathbb{Z}_{M_x}, n \in \mathbb{Z}_{M_y}. \tag{3.41}$$

It is obvious that DRR constraint degenerates to a CMC as $\zeta = 1$.

3.3.4 Optimization problem for scenario 1

In scenario 1, LEO SAT beampattern synthesis which aims to achieve broadened mainbeam while suppressing PSL with CMC/DRR constraints is formulated.

$$\begin{aligned}
&\text{minimize} && \max\{P_R \text{ in the out-of-beam areas}\} \text{ from } (3.3.2) && (3.42a)\\
&\text{subject to} && \mathrm{SNR} \ge \mathrm{SNR}_{\min} \text{ in the beam service areas from } (3.3.1) && (3.42b)\\
& && \text{weight coefficients satisfy CMC/DRR power constraint from } (3.3.3) && (3.42c)
\end{aligned}$$

We write problem 3.42 into its mathematical form.

$$\begin{aligned}
&\underset{\mu,\mathbf{X}\in\mathbb{C}^{M_x\times M_y}}{\text{minimize}} && \sup_{\theta\in[\theta_s,\theta_e],\phi\in[0,2\pi]} P_R(\mathbf{X},\theta,\phi) && (3.43a)\\
&\text{subject to} && \mathrm{SNR}(\mathbf{X},\theta,\phi) \ge \mathrm{SNR}_{\min}, \quad \forall\theta\in[0,\theta_{\mathrm{svc}}],\ \forall\phi\in[0,2\pi] && (3.43b)\\
& && \mu \le |[\mathbf{X}]_{m,n}| \le \mu\zeta, \quad m \in \mathbb{Z}_{M_x}, n \in \mathbb{Z}_{M_y}. && (3.43c)
\end{aligned}$$

doi:10.6342/NTU202303344

where $P_R(\mathbf{X}, \theta, \phi)$ is defined in (3.7), and $\text{SNR}(\mathbf{X}, \theta, \phi)$ is defined in (3.24).

Based on (3.38), (3.43a) is transformed to (3.44a). Based on (3.33), (3.43b) is transformed to (3.44b). Then, problem (3.43) is reformulated into the equivalent problem (3.44).

$$\underset{\mu\in\mathbb{R}_+, \mathbf{X}\in\mathbb{C}^{M_x\times M_y}}{\text{minimize}} \quad \sup_{\theta\in[\theta_s,\theta_e],\phi\in[0,2\pi]} \frac{|\tilde{\text{B}}(\mathbf{X}, \theta, \phi)|}{\sigma(\theta)} \tag{3.44a}$$

$$\text{subject to} \quad |\tilde{\text{B}}(\mathbf{X}, \theta, \phi)| \geq \alpha\sigma(\theta), \quad \forall\theta \in [0, \theta_{\text{svc}}],\ \phi \in [0, 2\pi] \tag{3.44b}$$

$$\mu \leq |[\mathbf{X}]_{m,n}| \leq \mu\zeta, \quad m \in \mathbb{Z}_{M_x}, n \in \mathbb{Z}_{M_y}., \tag{3.44c}$$

where $\tilde{\text{B}}(\mathbf{X}, \theta, \phi)$ is defined in (2.23), $\sigma(\theta)$ is defined in (3.16), and α is defined in (3.34).

3.3.5 Optimization problem for Scenario 2

In scenario 2, LEO SAT beampattern synthesis aims to achieve the Earth-coverage as the beampattern proposed in [11][24]. The SAT service angle θ_{svc} is set as SAT FoV angle θ_e obtained in (3.2). Since there are no sidelobe power leakage issue that should be considered in this scenario, the objective function is set to minimize the total transmitted power of satellite for power saving issue.

$$\text{minimize} \quad \text{Transmitted signal power} \tag{3.45a}$$

$$\text{subject to} \quad \text{SNR} \geq \text{SNR}_{\text{min}} \text{ in the beam service area} \tag{3.45b}$$

$$\text{weight coefficients satisfy CMC/DRR constraint} \tag{3.45c}$$

Under the assumption $\beta^2\mathbb{E}\{|s[k]|^2\} = 1$ and the service area mentioned in the next chapter (4.3), the transmitted signal power of the URA on a SAT is proportional to the

doi:10.6342/NTU202303344

total weight power $\sum_{m=0}^{M_x-1}\sum_{n=0}^{M_y-1}|[\mathbf{X}]_{m,n}|^2$. The proof is shown in A.1.

As a result, we could write problem 3.45 into its mathematical form.

$$\underset{\mu\in\mathbb{R}_+,\mathbf{X}\in\mathbb{C}^{M_x\times M_y}}{\text{minimize}} \quad \sum_{m=0}^{M_x-1}\sum_{n=0}^{M_y-1}|[\mathbf{X}]_{m,n}|^2 \tag{3.46a}$$

$$\text{subject to} \quad |\tilde{\mathbf{B}}(\mathbf{X},\theta,\phi)| \geq \alpha\sigma(\theta), \quad \forall\theta\in[0,\theta_{\text{svc}}],\ \forall\phi\in[0,2\pi] \tag{3.46b}$$

$$\mu \leq |[\mathbf{X}]_{m,n}| \leq \mu\zeta, \quad m\in\mathbb{Z}_{M_x}, n\in\mathbb{Z}_{M_y}, \tag{3.46c}$$

where the formulation of (3.46b) is based on (3.33).

doi:10.6342/NTU202303344

doi:10.6342/NTU202303344

Chapter 4 Proposed Algorithm

In this chapter, we describe the proposed algorithm for the main problem defined in (3.44) and (3.46). In section 4.1, we approximate the original URA problem with the combination of two sub-problems whose weight vector representing the ULAs on the x-axis and the y-axis. Since the reformulated ULA problems is nonconvex, we apply semi-definite relaxation (SDR) technique and solve the problem for scenario 1 with an iterative algorithm in section 4.2. Follow the same operation as that for scenario 1, we can reformulate the problems and solve the primal problem for scenario 2 in section 4.3. Finally, the ULA isoflux mask for the beampattern mainlobe is derived in section 4.4.

doi:10.6342/NTU202303344

4.1 Problem reformulations for scenario 1

In this section, the primal problem for scenario 1 (3.44) would be reformulated. After some transformations, the original service area would be covered by a URA transmit beamformer constructed with two ULA beamformers. We then focus on solving ULA problems. In the end of this section, a quadratic form of ULA problem is generated.

First, we rewrite problem 3.44 into its epigraph form

$$\underset{t\in\mathbb{R}_+,\mu\in\mathbb{R}_+,\mathbf{X}\in\mathbb{C}^{M_x\times M_y}}{\text{minimize}} \quad t \tag{4.1a}$$

$$\text{subject to} \quad |\tilde{\mathrm{B}}(\mathbf{X},\theta,\phi)| \le t\sigma(\theta), \quad \forall\theta\in[\theta_s,\theta_e],\ \forall\phi\in[0,2\pi] \tag{4.1b}$$

$$|\tilde{\mathrm{B}}(\mathbf{X},\theta,\phi)| \ge \alpha\sigma(\theta), \quad \forall\theta\in[0,\theta_{\text{svc}}],\ \forall\phi\in[0,2\pi] \tag{4.1c}$$

$$\mu \le |[\mathbf{X}]_{m,n}| \le \mu\zeta, \quad m\in\mathbb{Z}_{M_x}, n\in\mathbb{Z}_{M_y}, \tag{4.1d}$$

where $\tilde{\mathrm{B}}(\mathbf{X},\theta,\phi)$ is defined in (2.23), and α is defined in (3.34).

When it comes to larger antenna size, directly solving problem (4.1) which has $M_x \times M_y+2$ variables needs heavy computation. The original URA problem can be decomposed into two Uniform Linear Array (ULA) design problems [Cohen2019] [3][Albagory2022] [1][Frank2022] [7]. For the special case in which we have separable weightings

$$\mathbf{X} = \mathbf{x}\mathbf{y}^{\mathrm{T}} \text{ ,i.e, } [\mathbf{X}]_{m,n} = x_m y_n, m\in\mathbb{Z}_{M_x}, n\in\mathbb{Z}_{M_y}, \tag{4.2}$$

where $\mathbf{x}\in\mathbb{C}^{M_x}$ and $\mathbf{y}\in\mathbb{C}^{M_y}$. The total number of weights to be designed decrease from $M_x \times M_y + 2$ into $M_x + M_y + 2$. The beampattern of URA can be shown as the product of two ULA's beampattern.

doi:10.6342/NTU202303344

$$
\begin{aligned}
\tilde{\mathrm{B}}(\mathbf{X},\theta,\phi) &= \sum_{m=0}^{M_x-1}\sum_{n=0}^{M_y-1}[\mathbf{X}]^*_{m,n}e^{-j\pi f_c(\frac{m\sin(\theta)\cos(\phi)+n\sin(\theta)\sin(\phi)}{f_{\max}})} \\
&= \sum_{m=0}^{M_x-1}\sum_{n=0}^{M_y-1}(x_m y_n)^* e^{-j\pi f_c(\frac{m\sin(\theta)\cos(\phi)+n\sin(\theta)\sin(\phi)}{f_{\max}})} \\
&= \sum_{m=0}^{M_x-1} x_m^* e^{-j\pi m\sin(\theta)\cos(\phi)(\frac{f_c}{f_{\max}})} \sum_{n=0}^{M_y-1} y_n^* e^{-j\pi n\sin(\theta)\sin(\phi)(\frac{f_c}{f_{\max}})} \\
&= \sum_{m=0}^{M_x-1} x_m^* e^{-j\pi mu(\frac{f_c}{f_{\max}})} \sum_{n=0}^{M_y-1} y_n^* e^{-j\pi nv(\frac{f_c}{f_{\max}})} \\
&= \mathrm{B}(\mathbf{x},\vartheta_x)\mathrm{B}(\mathbf{y},\vartheta_y), \qquad (4.3)
\end{aligned}
$$

where $u \triangleq \sin(\theta)\cos(\phi) \in [-1,1]$, $v \triangleq \sin(\theta)\sin(\phi) \in [-1,1]$, $\vartheta_x \triangleq \sin^{-1}(u) \in [0,2\pi]$, and $\vartheta_y \triangleq \sin^{-1}(v) \in [0,2\pi]$. Note that the ϑ_x and ϑ_y are only used in ULA problems.

In our work, we decompose the URA beamformer design problem into two identical ULA beamformer design subproblems. We let the URA weight matrix $\mathbf{X}$ composed of two identical weight vectors $\mathbf{x}$.

$$\mathbf{X} = \mathbf{x}\mathbf{x}^{\mathrm{T}}. \qquad (4.4)$$

Then we can decompose the URA beampattern into the product of two identical ULA beampatterns at different angle.

$$\tilde{\mathrm{B}}(\mathbf{X},\theta,\phi) = \mathrm{B}(\mathbf{x},\vartheta_x)\mathrm{B}(\mathbf{x},\vartheta_y), \qquad (4.5)$$

doi:10.6342/NTU202303344

The problem 4.1 is converted into

$$\underset{t\in\mathbb{R}_+,\mu\in\mathbb{R}_+,\mathbf{x}\in\mathbb{C}^{M_x}}{\text{minimize}} \quad t \tag{4.6a}$$

$$\text{subject to} \quad |\mathrm{B}(\mathbf{x},\vartheta_x)||\mathrm{B}(\mathbf{x},\vartheta_y)| \le t\sigma(\theta), \quad \forall\theta\in[\theta_s,\theta_e], \quad \forall\phi\in[0,2\pi] \tag{4.6b}$$

$$|\mathrm{B}(\mathbf{x},\vartheta_x)||\mathrm{B}(\mathbf{x},\vartheta_y)| \ge \alpha\sigma(\theta), \quad \forall\theta\in[0,\theta_{\text{svc}}], \quad \forall\phi\in[0,2\pi] \tag{4.6c}$$

$$\mu \le |\mathbf{x}_m||\mathbf{x}_n| \le \mu\zeta, \quad m\in\mathbb{Z}_{M_x}, n\in\mathbb{Z}_{M_y}. \tag{4.6d}$$

- **Relationship between the mainlobe of URA beampattern and ULA beampattern**

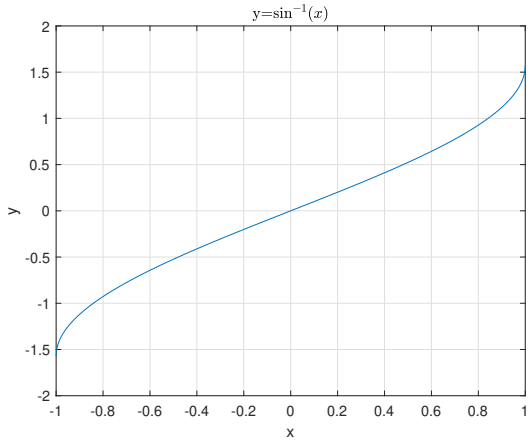

Figure 4.1: Arcsine function

The mainlobe of the URA beampattern is defined within the angular regions of $\theta \in [0,\theta_{\text{svc}}]$ with all $\phi\in[-\pi,\pi]$. Since $\vartheta_x = \sin^{-1}(\sin(\theta)\cos(\phi))$ and the arcsine function is increasing, the maximum value of ϑ_x is θ_{svc} when $\phi = 0$; the minimum value of ϑ_x is $-\theta_{\text{svc}}$ when $\phi = \pi$. Similar to ϑ_x, since $\vartheta_y = \sin^{-1}(\sin(\theta)\sin(\phi))$, the maximum value of ϑ_y is θ_{svc} when $\phi = \frac{\pi}{2}$; the minimum value of ϑ_y is $-\theta_{\text{svc}}$ when $\phi = -\frac{\pi}{2}$. As a consequence, to cover all θ for the mainlobe of the URA transmit beamformer, we should choose

$$\vartheta_x \in [-\theta_{\text{svc}},\theta_{\text{svc}}] \tag{4.7}$$

doi:10.6342/NTU202303344

as the mainlobe angular regions in ULA beamformer design subproblems. The relation between θ, ϕ, ϑ_x and ϑ_y is visualized in figure 4.2.

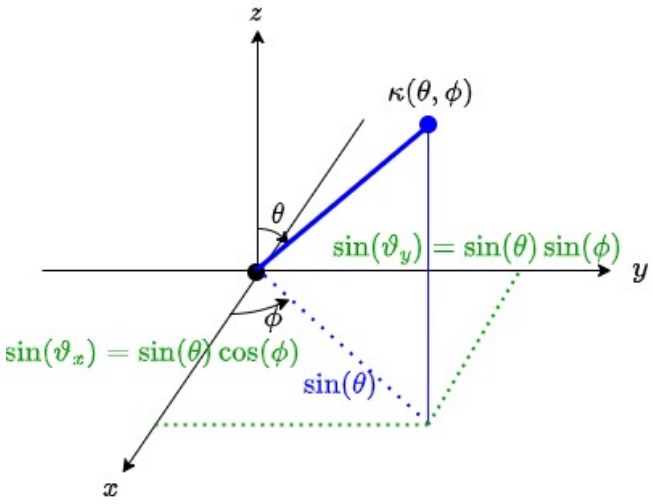

Figure 4.2: Spherical coordinate

We suppose the target is in the direction of the unit vector $\kappa(\theta, \phi)$. The projection of $\kappa(\theta, \phi)$ on the xy-plane is $\sin(\theta)$. Then, the projection on x-axis is $\sin(\vartheta_x) = \sin(\theta)\cos(\phi)$ and the the projection on the y-axis is $\sin(\vartheta_y) = \sin(\theta)\sin(\phi)$. Note that $\theta \in [0, \frac{\pi}{2}]$, $\phi \in [0, 2\pi]$, $\vartheta_x \in [-\frac{\pi}{2}, \frac{\pi}{2}]$, $\vartheta_y \in [-\frac{\pi}{2}, \frac{\pi}{2}]$.

Figure 4.3 is the top view of figure 4.2 as $\sin(\vartheta_x) = \sin(\vartheta_y) = \sin(\theta_{\text{svc}})$.

doi:10.6342/NTU202303344

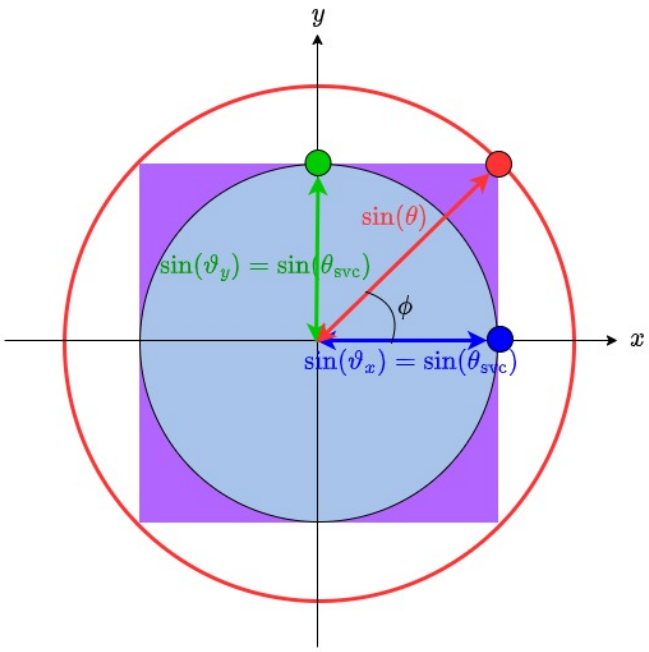

Figure 4.3: Top view of SAT service beam on Cartesian coordinate system

The service region designed in problem 4.6 is a circle on the Cartesian coordinate system, represented by the blue region in figure (4.3). However, if we decompose the URA beampattern design problem into two ULA beampattern design problems according to (4.5), the composite URA service region is rectangular which is the blue areas combined with the purple areas in figure (4.3). In the following, we will call the URA whose coverage is a circle circular-coverage URA, and call the square-coverage URA consisted with ULAs composite URA.

Then, the ULA mainlobe isoflux mask $\tilde{\sigma}(\vartheta)$ is obtained such that

$$\sqrt{\tilde{\sigma}(\vartheta_x)\tilde{\sigma}(\vartheta_y)} \geq \sigma(\theta), \quad \forall\theta \in [0, \theta_{\text{svc}}],\ \forall\phi \in [0, 2\pi], \tag{4.8}$$

where $\vartheta_x = \sin^{-1}(\sin(\theta)\cos(\phi))$, $\vartheta_y = \sin^{-1}(\sin(\theta)\sin(\phi))$.

doi:10.6342/NTU202303344

The ULA mask applied in this thesis is

$$\tilde{\sigma}(\vartheta_x) = \begin{cases} \sigma(\sin^{-1}(\sqrt{2}\sin(\vartheta_x))) & \text{if } \sin^{-1}(\sqrt{2}\sin(\vartheta_x)) \leq \theta_e \\ \frac{\sigma^2(\theta_e)}{\tilde{\sigma}(\vartheta_y)} & \text{if } \sin^{-1}(\sqrt{2}\sin(\vartheta_x)) \geq \theta_e \end{cases} \tag{4.9}$$

The derivation is shown in 4.4.

Then, if (4.10) holds, the mainlobe lower bound constraint (4.6c) will be satisfied. Namely, (4.10) is an over-designed constraint of (4.6c).

$$|\mathrm{B}(\mathbf{x}, \vartheta_x)||\mathrm{B}(\mathbf{x}, \vartheta_y)| \geq \alpha\sqrt{\tilde{\sigma}(\vartheta_x)\tilde{\sigma}(\vartheta_y)}, \quad \forall \vartheta_x, \vartheta_y \in [-\theta_{\text{svc}}, \theta_{\text{svc}}] \tag{4.10}$$

Since the two ULA beampatterns are identical, (4.10) can be reformulated as

$$|\mathrm{B}(\mathbf{x}, \vartheta_x)| \geq \sqrt{\alpha\tilde{\sigma}(\vartheta_x)}, \quad \forall \vartheta_x \in [-\theta_{\text{svc}}, \theta_{\text{svc}}] \tag{4.11}$$

- **Relation between the sidelobe of URA beampattern and ULA beampattern**

Based on the previous section, we realize that the service region of composite URA is a square, shown as the purple area in figure 4.4. As a result, the minimum angle among the sidelobe of URA beampattern which has circular-coverage areas should follow the below inequality,

$$\sin(\theta_s) > \sqrt{2}\sin(\theta_{\text{svc}}), \tag{4.12}$$

where θ_{svc} is the service angle of a composite URA.

doi:10.6342/NTU202303344

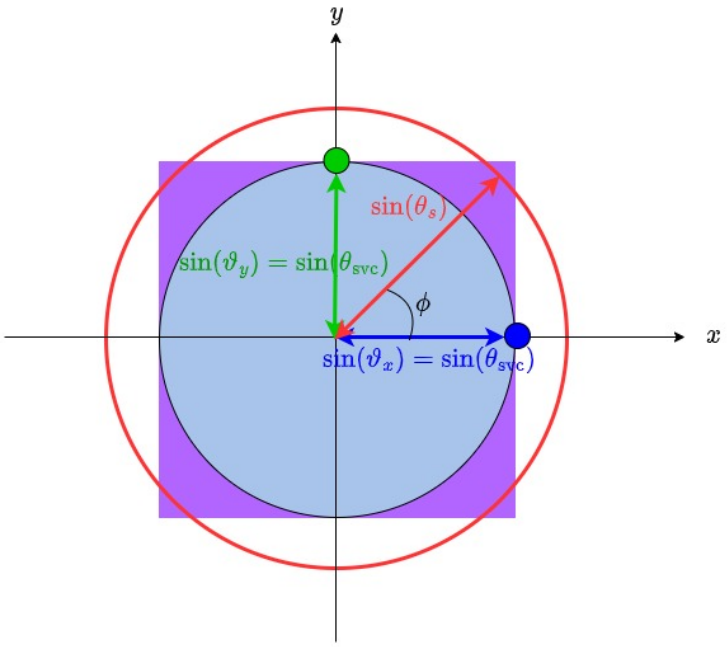

Figure 4.4: An improper θ_s of circular-coverage URA

As shown in figure 4.4, the mainlobe of a composite URA would be counted into the sidelobe of the circular-coverage URA if $\sin(\theta_s) \leq \sqrt{2}\sin(\theta_{\text{svc}})$.

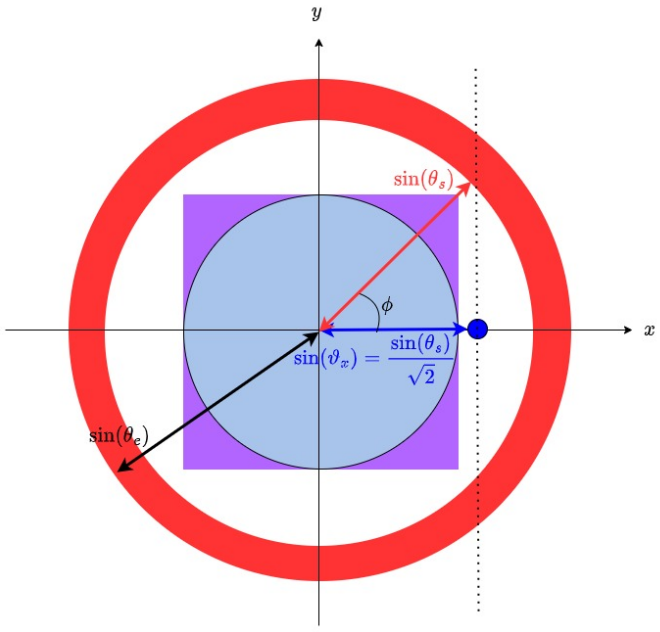

Figure 4.5: Relation between the sidelobe of circular-coverage URA and that of ULA

Therefore, the minimum sidelobe angle of ULA is when $\sin(\vartheta_x) = \frac{\sin(\theta_s)}{\sqrt{2}}$, where θ_s is

doi:10.6342/NTU202303344

the minimum sidelobe angle of circular-coverage URA. In this way, the sidelobe of ULA is defined in $\vartheta_x \in [-\theta_e, -\theta_s^*] \cup [\theta_s^*, \theta_e]$, where $\theta_s^* = \sin^{-1}(\frac{\sin(\theta_s)}{\sqrt{2}})$.

In (4.6b), we have

$$|\mathrm{B}(\mathbf{x}, \vartheta_x)||\mathrm{B}(\mathbf{x}, \vartheta_y)| \leq t\sigma(\theta), \quad \forall\theta \in [\theta_s, \theta_e], \quad \forall\phi \in [0, 2\pi]. \tag{4.13}$$

If we ensure

$$\sqrt{\bar{\sigma}(\vartheta_x)\bar{\sigma}(\vartheta_y)} \leq \sigma(\theta), \tag{4.14}$$

and

$$|\mathrm{B}(\mathbf{x}, \vartheta_x)||\mathrm{B}(\mathbf{x}, \vartheta_y)| \leq t\sqrt{\bar{\sigma}(\vartheta_x)\bar{\sigma}(\vartheta_y)}, \quad \forall\{\vartheta_x, \vartheta_y\} \in [\theta_s, \theta_e], \tag{4.15}$$

(4.6b) holds. In fact , we can choose

$$\bar{\sigma}(\vartheta_x) = \sigma(\vartheta_x) \tag{4.16}$$

Proof.

$$\bar{\sigma}(\vartheta_x) = \sigma(\vartheta_x) \tag{4.17}$$

$$= \sigma(\sin^{-1}(\sin(\theta)\cos(\phi))) \tag{4.18}$$

$$\downarrow\ \sigma(\cdot) \text{ and arcsine are increasing in the function domain} \tag{4.19}$$

$$\leq \sigma(\sin^{-1}(\sin(\theta))) = \sigma(\theta) \tag{4.20}$$

□

Because the composite URA is consisted with two identical beamformers. The side-

doi:10.6342/NTU202303344

lobe constraint (4.6b) turns into

$$|\mathrm{B}(\mathbf{x}, \vartheta_x)| \leq \sqrt{t\sigma(\vartheta_x)}, \quad \forall \vartheta_x \in [-\theta_e, -\theta_s^*] \cup [\theta_s^*, \theta_e] \tag{4.21}$$

Combined with (4.11) and (4.21), an approximated problems are reformulated from problem 4.6.

$$\underset{t\in\mathbb{R}_+, \mu\in\mathbb{R}_+, \mathbf{x}\in\mathbb{C}^{M_x}}{\text{minimize}} \quad \sqrt{t} \tag{4.22a}$$

$$\text{subject to} \quad |\mathrm{B}(\mathbf{x}, \vartheta_x)| \leq \sqrt{t\sigma(\vartheta_x)}, \quad \forall \vartheta_x \in [-\theta_e, -\theta_s^*] \cup [\theta_s^*, \theta_e] \tag{4.22b}$$

$$|\mathrm{B}(\mathbf{x}, \vartheta_x)| \geq \sqrt{\alpha\tilde{\sigma}(\vartheta_x)}, \quad \forall \vartheta_x \in [-\theta_{\text{svc}}, \theta_{\text{svc}}] \tag{4.22c}$$

$$\sqrt{\mu} \leq |\mathbf{x}_m| \leq \sqrt{\mu\zeta}, \quad m \in \mathbb{Z}_{M_x} \tag{4.22d}$$

Recall (2.18), $\mathrm{B}(\mathbf{x}, \vartheta_x) = \mathbf{x}^H \mathbf{a}(\vartheta_x)$. $|\mathrm{B}(\mathbf{x}, \vartheta_x)|^2 = \mathbf{x}^H \mathbf{a}(\vartheta_x)\mathbf{a}^H(\vartheta_x)\mathbf{x}$. We define

$$\mathbf{A}(\vartheta_x) = \mathbf{a}(\vartheta_x)\mathbf{a}^H(\vartheta_x), \tag{4.23}$$

$\Rightarrow |\mathrm{B}(\mathbf{x}, \vartheta_x)|^2 = \mathbf{x}^H \mathbf{A}(\vartheta_x)\mathbf{x}$. Besides, we can rewrite x_m as $\mathbf{e}_m^H\mathbf{x}$, where $\mathbf{e}_m(i) = \begin{cases} 1 & \text{if } i = m \\ 0 & \text{else} \end{cases}$, $\mathbf{e}_m \in \mathbb{R}^{M_x}$. If we define $\mathbf{E}_m = \mathbf{e}_m\mathbf{e}_m^H$,

$$|x_m|^2 = \mathbf{x}^H \mathbf{e}_m \mathbf{e}_m^H \mathbf{x} = \mathbf{x}^H \mathbf{E}_m \mathbf{x} \tag{4.24}$$

doi:10.6342/NTU202303344

Then we can transform problem 4.22 into problem 4.25 as its quadratic form.

$$\underset{t\in\mathbb{R}_+,\mu\in\mathbb{R}_+,\mathbf{x}\in\mathbb{C}^{M_x}}{\text{minimize}} \quad t \tag{4.25a}$$

$$\text{subject to} \quad \mathbf{x}^H\mathbf{A}(\vartheta_x)\mathbf{x} \le t\sigma(\vartheta_x), \quad \forall\vartheta_x \in [-\theta_e, -\theta_s^*] \cup [\theta_s^*, \theta_e] \tag{4.25b}$$

$$\mathbf{x}^H\mathbf{A}(\vartheta_x)\mathbf{x} \ge \alpha\tilde{\sigma}(\vartheta_x), \quad \forall\vartheta_x \in [-\theta_{\text{svc}}, \theta_{\text{svc}}] \tag{4.25c}$$

$$\mu \le \mathbf{x}^H\mathbf{E}_m\mathbf{x} \le \mu\zeta, \quad m \in \mathbb{Z}_{M_x} \tag{4.25d}$$

4.2 Proposed algorithm for scenario 1

In this section, semidifinite relaxation (SDR) with rank 1 constraint and Dattorro iterative algorithm is used to deal with the nonconvex problem. Semidifinite Relaxation (SDR) is useful for many nonconvex quadratically constrained quadratic programs (QCQPs)[16]. One of the basic QCQP form is shown as

$$\begin{aligned} \underset{\mathbf{x}\in\mathbb{R}^M}{\text{minimize}} \quad & \mathbf{x}^T\mathbf{C}\mathbf{x} \\ \text{subject to} \quad & \mathbf{x}^T\mathbf{F}_i\mathbf{x} \ge f_i, \quad i \in \mathbb{Z}_p \\ & \mathbf{x}^T\mathbf{G}_i\mathbf{x} = g_i, \quad i \in \mathbb{Z}_q \end{aligned}$$

In fact, if the $\mathbf{C}$, $\mathbf{F}_i$, $\mathbf{G}_i$ in the above QCQP are Hermitian matrices, we can extend QCQP to complex QCQP where the complex solution $\mathbf{x}$ is obtainable.

$$\begin{aligned} \underset{\mathbf{x}\in\mathbb{C}^M}{\text{minimize}} \quad & \mathbf{x}^H\mathbf{C}\mathbf{x} \\ \text{subject to} \quad & \mathbf{x}^H\mathbf{F}_i\mathbf{x} \ge f_i, \quad i \in \mathbb{Z}_p \\ & \mathbf{x}^T\mathbf{G}_i\mathbf{x} = g_i, \quad i \in \mathbb{Z}_q \end{aligned}$$

doi:10.6342/NTU202303344

Obviously, problem 4.25 is a complex QCQP. Derived from (4.25c), we could observe that $\mathbf{x}^H\mathbf{A}(\vartheta_x)\mathbf{x} = \mathrm{Tr}(\mathbf{x}^H\mathbf{A}(\vartheta_x)\mathbf{x}) = \mathrm{Tr}(\mathbf{x}\mathbf{x}^H\mathbf{A}(\vartheta_x))$. If we define $\tilde{\mathbf{X}} = \mathbf{x}\mathbf{x}^H$, (4.25c) turns into

$$\mathrm{Tr}(\tilde{\mathbf{X}}\mathbf{A}(\vartheta_x)) \geq \alpha\tilde{\sigma}(\vartheta_x), \quad \forall\vartheta_x \in [-\theta_{\text{svc}}, \theta_{\text{svc}}], \tag{4.28}$$

Meanwhile, in the original problem, we must ensure $\tilde{\mathbf{X}} = \mathbf{x}\mathbf{x}^H$. Hence, the following equation should be also satisfied.

$$\mathrm{rank}(\tilde{\mathbf{X}}) = 1, \ \tilde{\mathbf{X}} \in \mathbb{R}_+ \tag{4.29}$$

We can transform (4.25b), (4.25c),and (4.25d) in the same way. Thus, a transformed problem is formulated.

$$\underset{t\in\mathbb{R}_+,\mu\in\mathbb{R}_+,\tilde{\mathbf{X}}\in\mathbb{H}_+^{M_x}}{\text{minimize}} \quad t \tag{4.30a}$$

$$\text{subject to} \quad \mathrm{Tr}(\tilde{\mathbf{X}}\mathbf{A}(\vartheta_x)) \leq t\sigma(\vartheta_x), \quad \forall\vartheta_x \in [-\theta_e, -\theta_s^*] \cup [\theta_s^*, \theta_e] \tag{4.30b}$$

$$\mathrm{Tr}(\tilde{\mathbf{X}}\mathbf{A}(\vartheta_x)) \geq \alpha\tilde{\sigma}(\vartheta_x), \quad \forall\vartheta_x \in [-\theta_{\text{svc}}, \theta_{\text{svc}}] \tag{4.30c}$$

$$\mu \leq \mathrm{Tr}(\tilde{\mathbf{X}}\mathbf{E}_m) \leq \mu\zeta, \quad m \in \mathbb{Z}_{M_x} \tag{4.30d}$$

$$\mathrm{rank}(\tilde{\mathbf{X}}) = 1 \tag{4.30e}$$

The constraints in problem 4.30 are convex except for constraint (4.30e). To solve this nonconvex problem and obtain a rank-1 matrix, Dattorro iterative algorithm[4] is applied in this thesis. CVX [9] is used to construct and solve a convex program.

doi:10.6342/NTU202303344

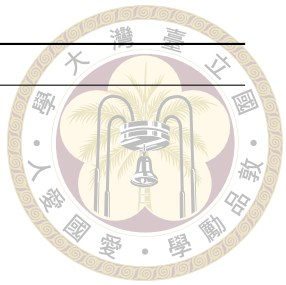

Algorithm 1 Dattorro Iterative Algorithm for scenario 1

Input: ρ, $\varepsilon_{\text{rank}}$;

Output: $\mathbf{x}$;

$\mathbf{V}^{(0)} \leftarrow \mathbf{0}$ and $\psi \leftarrow 0$

repeat

  solve **Problem** 4.31 by CVX

  if Problem 4.31 is infeasible **then**

    return infeasible

  end if

  Perform eigen-decomposition on $\mathbf{X}^{(\psi)}$: $\mathbf{X}^{(\psi)} = \tilde{\mathbf{U}}^{(\psi)}\mathbf{D}^{(\psi)}(\tilde{\mathbf{U}}^{(\psi)})^H$, where

  $\tilde{\mathbf{U}}^{(\psi)} = [\mathbf{u}_0^{(\psi)}\ \mathbf{u}_1^{(\psi)}\ \ldots\ \mathbf{u}_{M_x-1}^{(\psi)}]$

  $\mathbf{U}^{(\psi)} = [\mathbf{u}_1^{(\psi)}\ \ldots\ \mathbf{u}_{M_x-1}^{(\psi)}]$

  $\mathbf{V}^{(\psi+1)} = \mathbf{U}^{(\psi)}(\mathbf{U}^{(\psi)})^H$

  $\sigma_0 = [\mathbf{D}^{(\psi)}]_{0,0}$, $\sigma_1 = [\mathbf{D}^{(\psi)}]_{1,1}$

  Update ρ

  $\psi \leftarrow \psi + 1$

until $\sigma_1/\sigma_0 \leq \varepsilon_{\text{rank}}$

Obtain $\mathbf{x} = \sqrt{\sigma_0}\mathbf{u}_0$

This algorithm perform eigenvalue decomposition to achieve a matrix whose ratio of second largest eigenvalue to largest eigenvalue as low as possible. As the ratio lower than $\varepsilon_{\text{rank}}$, we can assume this matrix satisfy rank-1 constraint. If the stopping criterion not satisfied, we collect the eigenvectors from the second largest to the smallest eigenvalue. In the next iteration, we tend to obtain a $\mathbf{X}$ independent of these extracted eigenvectors. This independency can be achieved from the objective function of problem 4.31.

doi:10.6342/NTU202303344

$$\underset{t\in\mathbb{R}_+,\mu\in\mathbb{R}_+,\tilde{\mathbf{X}}^{(\psi)}\in\mathbb{H}_+^{M_x}}{\text{minimize}} \quad t+\rho\text{Tr}(\tilde{\mathbf{X}}^{(\psi)}\mathbf{V}^{(\psi-1)}) \tag{4.31a}$$

$$\text{subject to} \quad \text{Tr}(\tilde{\mathbf{X}}^{(\psi)}\mathbf{A}(\vartheta_x)) \le t\sigma(\vartheta_x), \quad \forall\vartheta_x\in[-\theta_e,-\theta_s^*]\cup[\theta_s^*,\theta_e] \tag{4.31b}$$

$$\text{Tr}(\tilde{\mathbf{X}}^{(\psi)}\mathbf{A}(\vartheta_x)) \ge \alpha\tilde{\sigma}(\vartheta_x), \quad \forall\vartheta_x\in[-\theta_{\text{svc}},\theta_{\text{svc}}] \tag{4.31c}$$

$$\mu \le \text{Tr}(\tilde{\mathbf{X}}^{(\psi)}\mathbf{E}_m) \le \mu\zeta, \quad m\in\mathbb{Z}_{M_x} \tag{4.31d}$$

The ρ in objective function is to control the priority to either rank-1 control or PSL control. If ρ is large, we tend to find a matrix satisfying rank-1 constraint more and accelerate the convergence; in the other hand, if ρ is small, the required iteration number increase, but the algorithm may converge to a $\mathbf{x}$ which can achieve a lower PSL. In [algorithm 1] 1, $\rho\in\mathbb{Z}$ and $\varepsilon_{\text{rank}}$ is a extremely small number.

4.2.1 Initial point selection

Initial point of the Dattorro algorithm $\mathbf{x}_{\text{init}}$ is selected as the beamforming coefficients proposed in [6] which has a controllable mainbeam beamwidth and a low sidelobe.

4.2.2 Update of ρ

ρ would not change unless $\frac{\sigma_0^{(\psi)}}{\sigma_1^{(\psi)}}-\frac{\sigma_0^{(\psi-1)}}{\sigma_1^{(\psi-1)}}\le\kappa$, then $\rho^{(\psi)}=\rho^{(\psi-1)}\times(1+p)$, where κ and p are positive numbers. This is a relatively passive method that only when the problem converges slowly or even stop converging that we enhance the rank control.

doi:10.6342/NTU202303344

4.3 Problem algorithm for scenario 2

Recall the primal problem for scenario 2 (3.46)

$$\underset{\mu\in\mathbb{R}_+,\mathbf{X}\in\mathbb{C}^{M_x\times M_y}}{\text{minimize}} \quad \sum_{m=0}^{M_x-1}\sum_{n=0}^{M_y-1} |[\mathbf{X}]_{m,n}|^2 \tag{4.32a}$$

$$\text{subject to} \quad |\tilde{\mathrm{B}}(\mathbf{X},\theta,\phi)| \geq \alpha\sigma(\theta), \quad \forall\theta\in[0,\theta_{\text{svc}}],\ \forall\phi\in[0,2\pi] \tag{4.32b}$$

$$\mu \leq |[\mathbf{X}]_{m,n}| \leq \mu\zeta, \quad m\in\mathbb{Z}_{M_x}, n\in\mathbb{Z}_{M_y}, \tag{4.32c}$$

Follow the variable transformation from θ and ϕ into ϑ_x and ϑ_y, where $\vartheta_x = \sin^{-1}(\sin(\theta)\cos(\phi))$, $\vartheta_y = \sin^{-1}(\sin(\theta)\sin(\phi))$, and $\mathbf{X} = \mathbf{x}\mathbf{x}^T$, we can turn problem 4.32 into problem 4.33

$$\underset{\mu\in\mathbb{R}_+,\mathbf{x}\in\mathbb{C}^{M_x}}{\text{minimize}} \quad \sum_{m=0}^{M_x-1}\sum_{n=0}^{M_x-1} |\mathbf{x}_m|^2|\mathbf{x}_n|^2 \tag{4.33a}$$

$$\text{subject to} \quad |\mathrm{B}(\mathbf{x},\vartheta_x)||\mathrm{B}(\mathbf{x},\vartheta_y)| \geq \alpha\sigma(\theta), \quad \forall\theta\in[0,\theta_{\text{svc}}], \quad \forall\phi\in[0,2\pi] \tag{4.33b}$$

$$\mu \leq |\mathbf{x}_m||\mathbf{x}_n| \leq \mu\zeta, \quad m,n\in\mathbb{Z}_{M_x}. \tag{4.33c}$$

After replacing the $\sigma(\theta)$ in (4.33b) with $\sqrt{\tilde{\sigma}(\vartheta_x)\tilde{\sigma}(\vartheta_y)}$, we can formulate an over-designed problem (4.34), where $\sqrt{\tilde{\sigma}(\vartheta_x)\tilde{\sigma}(\vartheta_y)} \geq \sigma(\theta)$

$$\underset{\mu\in\mathbb{R}_+,\mathbf{x}\in\mathbb{C}^{M_x}}{\text{minimize}} \quad \sum_{m=0}^{M_x-1} |\mathbf{x}_m|^2 \sum_{n=0}^{M_x-1} |\mathbf{x}_n|^2 \tag{4.34a}$$

$$\text{subject to} \quad |\mathrm{B}(\mathbf{x},\vartheta_x)||\mathrm{B}(\mathbf{x},\vartheta_y)| \geq \alpha\sqrt{\tilde{\sigma}(\vartheta_x)\tilde{\sigma}(\vartheta_y)}, \quad \forall\vartheta_x,\vartheta_y\in[-\theta_{\text{svc}},\theta_{\text{svc}}] \tag{4.34b}$$

$$\mu \leq |\mathbf{x}_m||\mathbf{x}_n| \leq \mu\zeta, \quad m,n\in\mathbb{Z}_{M_x}. \tag{4.34c}$$

doi:10.6342/NTU202303344

We can turns (4.34) into a ULA problem

$$\underset{\mu\in\mathbb{R}_+,\mathbf{x}\in\mathbb{C}^{M_x}}{\text{minimize}} \quad \sum_{m=0}^{M_x-1} |\mathbf{x}_m|^2 \tag{4.35a}$$

$$\text{subject to} \quad |\mathrm{B}(\mathbf{x},\vartheta_x)| \geq \sqrt{\alpha\tilde{\sigma}(\vartheta_x)}, \quad \forall\vartheta_x \in [-\theta_{\text{svc}},\theta_{\text{svc}}] \tag{4.35b}$$

$$\sqrt{\mu} \leq |\mathbf{x}_m| \leq \sqrt{\mu\zeta}, \quad m \in \mathbb{Z}_{M_x} \tag{4.35c}$$

After applying quadratic transform and trace transform mentioned in problem 4.25 and 4.30, problem 4.36 is reformulated as

$$\underset{\mu\in\mathbb{R}_+,\tilde{\mathbf{X}}\in\mathbb{H}_+^{M_x}}{\text{minimize}} \quad \mathrm{Tr}(\tilde{\mathbf{X}}) \tag{4.36a}$$

$$\text{subject to} \quad \mathrm{Tr}(\tilde{\mathbf{X}}\mathbf{A}(\vartheta_x)) \geq \alpha\tilde{\sigma}(\vartheta_x), \quad \forall\vartheta_x \in [-\theta_{\text{svc}},\theta_{\text{svc}}] \tag{4.36b}$$

$$\mu \leq \mathrm{Tr}(\tilde{\mathbf{X}}\mathbf{E}_m) \leq \mu\zeta, \quad m \in \mathbb{Z}_{M_x}, \tag{4.36c}$$

$$\mathrm{rank}(\tilde{\mathbf{X}}) = 1 \tag{4.36d}$$

where $\mathbf{A}(\vartheta_x)$ is defined in (4.23) and $\mathbf{E}_m$ is defined in (4.24). As same as scenario 1, we apply Dattorro iterative algorithm to the nonconvex problem.

doi:10.6342/NTU202303344

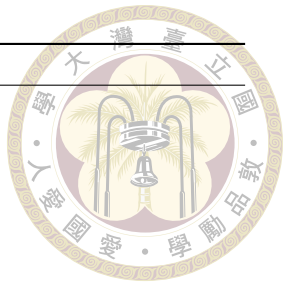

Algorithm 2 Dattorro Iterative Algorithm for scenario 2

Input: ρ, $\varepsilon_{\text{rank}}$;

Output: $\mathbf{x}$;

$\mathbf{V}^{(0)} \leftarrow \mathbf{0}$ and $\psi \leftarrow 0$

repeat

  solve **Problem** 4.37 by CVX

  if Problem 4.37 is infeasible **then**

    return infeasible

  end if

  Perform eigen-decomposition on $\mathbf{X}^{(\psi)}$: $\mathbf{X}^{(\psi)} = \tilde{\mathbf{U}}^{(\psi)}\mathbf{D}^{(\psi)}(\tilde{\mathbf{U}}^{(\psi)})^H$, where

  $\tilde{\mathbf{U}}^{(\psi)} = [\mathbf{u}_0^{(\psi)}\ \mathbf{u}_1^{(\psi)}\ \ldots\ \mathbf{u}_{M_x-1}^{(\psi)}]$

  $\mathbf{U}^{(\psi)} = [\mathbf{u}_1^{(\psi)}\ \ldots\ \mathbf{u}_{M_x-1}^{(\psi)}]$

  $\mathbf{V}^{(\psi+1)} = \mathbf{U}^{(\psi)}(\mathbf{U}^{(\psi)})^H$

  $\sigma_0 = [\mathbf{D}^{(\psi)}]_{0,0}$, $\sigma_1 = [\mathbf{D}^{(\psi)}]_{1,1}$

  Update ρ

  $\psi \leftarrow \psi + 1$

until $\sigma_1/\sigma_0 \leq \varepsilon_{\text{rank}}$

Obtain $\mathbf{x} = \sqrt{\sigma_0}\mathbf{u}_0$

In each iteration, the Dattorro iterative algorithm solves problem (4.37)

$$\underset{\mu\in\mathbb{R}_+,\tilde{\mathbf{X}}^{(\psi)}\in\mathbb{H}_+^{M_x}}{\text{minimize}} \quad \text{Tr}(\tilde{\mathbf{X}}^{(\psi)}) + \rho\text{Tr}(\tilde{\mathbf{X}}^{(\psi)}\mathbf{V}^{(\psi-1)}) \tag{4.37a}$$

$$\text{subject to} \quad \text{Tr}(\tilde{\mathbf{X}}^{(\psi)}\mathbf{A}(\vartheta_x)) \geq \alpha\tilde{\sigma}(\vartheta_x), \quad \forall\vartheta_x \in [-\theta_{\text{svc}}, \theta_{\text{svc}}] \tag{4.37b}$$

$$\mu \leq \text{Tr}(\tilde{\mathbf{X}}^{(\psi)}\mathbf{E}_m) \leq \mu\zeta, \quad m \in \mathbb{Z}_{M_x} \tag{4.37c}$$

doi:10.6342/NTU202303344

4.4 ULA mainlobe isoflux mask derivation

Recall (3.16), the URA isoflux mask is

$$\sigma(\theta) = \frac{\left[(h+R_E)\cos(\theta) - \sqrt{R_E^2 - (h+R_E)^2\sin^2(\theta)}\right]}{h}, \tag{4.38}$$

where h is the satellite altitude, R_E is the radius of the Earth, and θ is the slant angle.

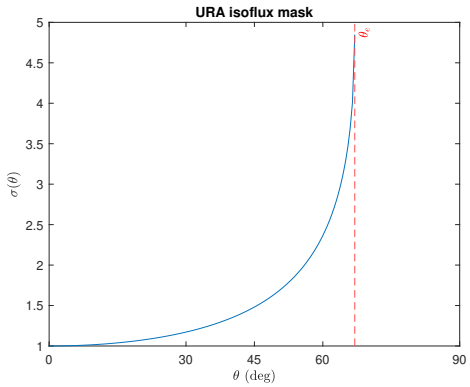

Figure 4.6: URA Isoflux mask

As shown in figure 4.6, $\sigma(\theta)$ is non-decreasing for $\theta \in [0, \theta_e]$.

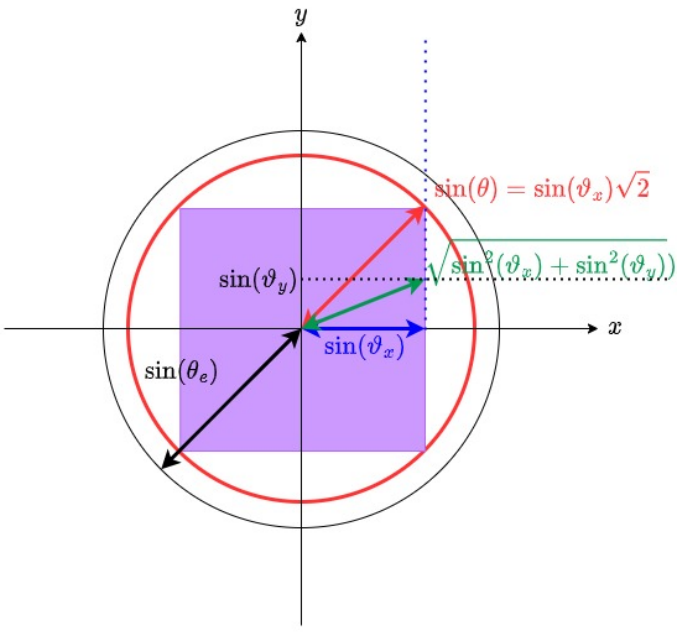

Figure 4.7: Isoflux mask example 1

doi:10.6342/NTU202303344

Under the inference

$$\min\{\tilde{\sigma}(\vartheta_x)\tilde{\sigma}(\vartheta_y) - \sigma^2(\theta)\} \text{ happens when } \vartheta_x = \vartheta_y, \tag{4.39}$$

the azimuth angle ϕ is implied to be $45°$. In this way, when designing a ULA beampattern at angle ϑ_x, we should consider the isoflux mask at angle $\theta = \sin^{-1}(\sqrt{2}\sin(\vartheta_x))$. Therefore, the ULA isoflux mask at angle ϑ_x is formulated as follows

$$\tilde{\sigma}(\vartheta_x) = \sigma(\theta) = \sigma(\sin^{-1}(\sqrt{2}\sin(\vartheta_x))). \tag{4.40}$$

We apply numerical analysis to prove the correctness of the inference (4.39). We fixed ϑ_x and change ϕ to generate corresponding ϑ_y and θ based on (4.40). Below is the result of $(\tilde{\sigma}(\vartheta_x)\tilde{\sigma}(\vartheta_y) - \sigma^2(\theta))$. The x-axis represents ϕ in degree unit and we sample ϕ with $0.001°$. It is shown that if $\tilde{\sigma}(\vartheta)$ is defined as (4.40), we are able to claim

$$\tilde{\sigma}(\vartheta_x)\tilde{\sigma}(\vartheta_y) \geq \sigma^2(\theta)), \quad \forall\theta \in [0, \theta_{\text{svc}}], \quad \forall\phi \in [-\pi, \pi] \tag{4.41}$$

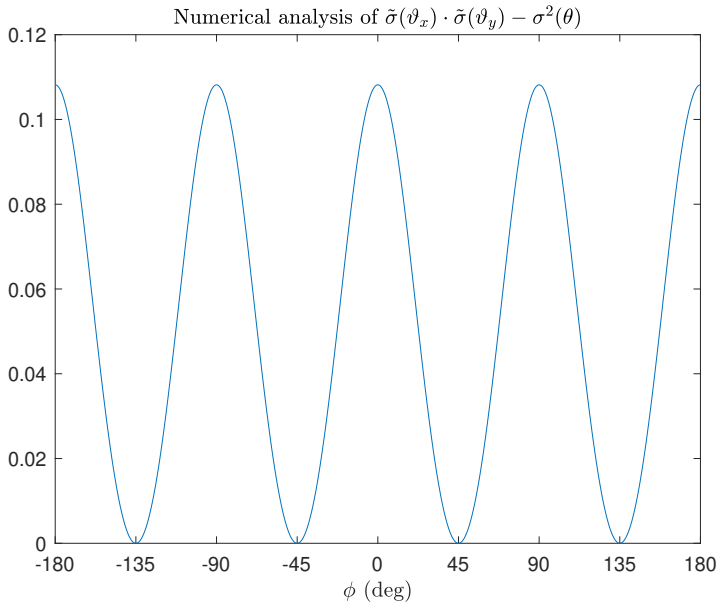

Figure 4.8: Numerical analysis

doi:10.6342/NTU202303344

However, when $\sin^{-1}(\sqrt{2}\sin(\vartheta_x)) > \theta_e$, the square root value in $\sigma(\theta)$, $\sqrt{R_E^2 - (h+R_E)^2\sin^2(\theta)}$, is not a real number.

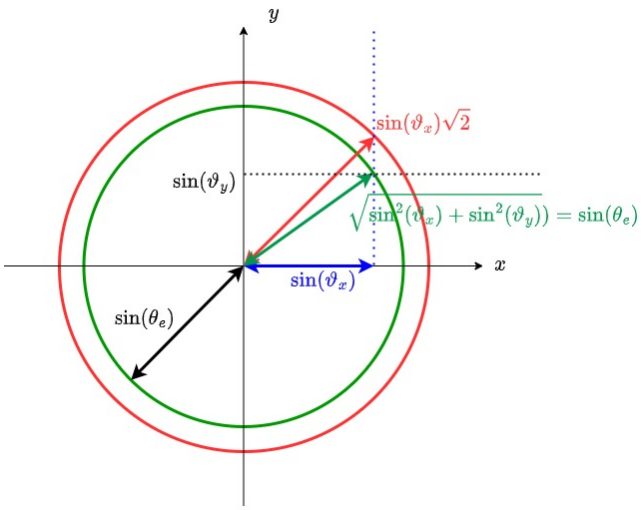

Figure 4.9: Isoflux mask example 2

As shown in figure 4.9, the achievable $\sin(\theta) = \sin(\theta_e)$ is described by the green arrow. The projection of $\sin(\theta_e)$ on the y-axis is $\sin(\vartheta_y)$. Since $\sqrt{2}\sin(\vartheta_y) \leq \sin(\theta_e)$ is ensured, the value of $\tilde{\sigma}(\vartheta_y)$ can be derived from (4.40). To meet $\sqrt{\tilde{\sigma}(\vartheta_y)\tilde{\sigma}(\vartheta_x)} \geq \sigma(\theta_e)$ mentioned in (4.8), we let

$$\tilde{\sigma}(\vartheta_x) = \frac{\sigma^2(\theta_e)}{\tilde{\sigma}(\vartheta_x)}. \tag{4.42}$$

Therefore, $\tilde{\sigma}(\vartheta_x)$ can be designed as

$$\tilde{\sigma}(\vartheta_x) = \begin{cases} \sigma(\sin^{-1}(\sqrt{2}\sin(\vartheta_x))) & \text{if } \sin^{-1}(\sqrt{2}\sin(\vartheta_x)) \leq \theta_e \\ \frac{\sigma^2(\theta_e)}{\tilde{\sigma}(\vartheta_y)} & \text{if } \sin^{-1}(\sqrt{2}\sin(\vartheta_x)) > \theta_e \end{cases} \tag{4.43}$$

doi:10.6342/NTU202303344

Chapter 5 Simulation

In this chapter, we refer to the specifications applied in modern SatComm. We would check if the signals transmitted under these specifications are narrowband or not. Then, the field of view (FoV), mainbeam beamwidth, mainlobe lower bound, free-space propagation loss are calculated subsequently based on the SatComm specifications. The simulation results for scenario 1 and scenario 2 are shown in section 5.2. Besides, we compare the results of proposed method to those in previous works. In section 5.3, it is shown that if the mainbeam is wider, we can obtain a larger average channel capacity.

5.1 LEO SAT system setups

In this section, we derive the parameters applied in our optimization problem design. In subsection 5.1.1, we show the specifications written in the modern SatComm documents. Some basic parameters are also derived. In subsection 5.1.2, the lower bound of mainlobe is derived to satisfy required channel capacity.

doi:10.6342/NTU202303344

5.1.1 LEO SAT system parameters

Parameter	Symbol	Value	Units	Reference
SAT altitude	h	550	km	SpaceX [5]
Earth radius	R_e	6370	km	
Carrier frequency (SAT to UE)	f_c	12	GHz	SpaceX [5]
Channel bandwidth	$f_{\text{BW}_{\text{ch}}}$	250	MHz	SpaceX [5]
Frequency reuse factor	k_f	3		3GPP TR16 [21]
Signal bandwidth	f_{BW}	80	MHz	
Cable loss	$L_{c,T,\text{dB}}$	0	[dB]	
Atmospheric path loss	$L_{\text{a,dB}}$	0.5	[dB]	3GPP TR15 [20]
Shadowing loss	$L_{\text{sm,dB}}$	0	[dB]	LOS case in 3GPP TR15 [20]
Scintillation loss	$L_{\text{sl,dB}}$	0.3	[dB]	3GPP TR15 [20]
Number of receive antennas	$N_{a,R}$	49×49		SpaceX patent [14]
Antenna temperature	$T_{a,R}$	150	[K]	3GPP TR15 [20]
Noise figure	N_f	1.2	[dB]	3GPP TR15 [20]
Boltzman constant	k_{dB}	-228.6	[dBW/K/Hz]	
Standard temperature	T_0	290	[K]	

Table 5.1: SAT scenario for link budget evaluations

Note that $L_{c,T,\text{dB}} = 10 \times \log_{10}(L_{c,T})$, $L_{\text{a,dB}} = 10 \times \log_{10}(L_{\text{a}})$, $L_{\text{sm,dB}} = 10 \times \log_{10}(L_{\text{sm}})$, $L_{\text{sl,dB}} = 10 \times \log_{10}(L_{\text{sl}})$, $k_{\text{dB}} = 10 \times \log_{10}(k)$.

To determine whether the transmitted signals is narrowband, we recall the definition of the fractional bandwidth (2.4).

$$f_{\text{FB}} = \frac{f_h - f_l}{f_h + f_l} \times 100\% \tag{5.1}$$

The highest frequency $f_h = 12040$MHz and the lowest frequency $f_l = 11960$MHz. The

doi:10.6342/NTU202303344

fractional bandwidth is $\frac{80}{12000} \times 100\% = 0.67\%$. Since the transmitted signal is narrowband, the URA system model in figure 2.3 is usable.

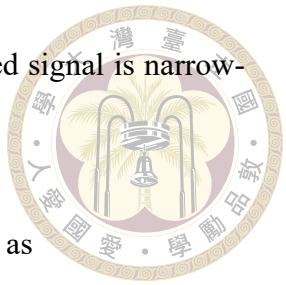

According to (3.2), the boundary angle of FoV can be calculated as

$$\theta_e = \sin^{-1}(\frac{R_E}{h + R_E}) \approx 67^\circ \tag{5.2}$$

5.1.2 Mainlobe lower bound

Assume that we would like to achieve a channel capacity larger than 150 [Mbps] under the signal bandwidth of 250 [MHz] with the frequency reuse factor $k_f = 3$. Accroding to Shannon capacity theorem,

$$C = f_{\text{BW}} \log_2(1 + \text{SNR}), \tag{5.3}$$

SNR $= 5$ [dB] enables us to achieve channel capacity of 171.5 [Mbps], which surpasses the required channel capacity.

According to (3.30), the relation between SNR and the beampattern is

$$5 \leq 10 \log_{10} \left(\frac{|\text{B}(\mathbf{X}, \theta, \phi)|^2 G_R}{\sigma^2(\theta) k T_{\text{sys}} f_{\text{BW}} L_0} \right), \tag{5.4}$$

where T_{sys} can be derived from (3.23) and $L_0 = L_{\text{c,T}} L_{\text{c,R}} L_{\text{a}} L_{\text{sm}} L_{\text{sl}} (\frac{4 \times 550 \times 10^3 \times \pi}{\lambda})^2$, written in (3.19). Since the transmitted signal is narrowband, we can approximate λ with λ_c, where λ_c is the wavelength of carrier frequency f_c. $\lambda_c = \frac{3 \times 10^8}{12 \times 10^9} = 0.025[m]$ Therefore, the path loss of the shortest path is $L_{\text{fs0}} = \frac{2.2 \times \pi \times 10^6}{0.025}$. It is equivalent to 168.8616 dB. According to the table 5.1, $T_{\text{sys}} = 242.2945$. Therefore, $10 \log_{10}(k T_{\text{sys}} f_{\text{BW}} L_0) = -228.6 + 23.8434 + 79.0309 + 169.6327 = 43.907$ dB

doi:10.6342/NTU202303344

$G_R = N_{a,R} \times G_{R,e}$. Based on the setup, $N_{a,R} = 49 \times 49$. We also assume $G_{R,e}$ to be 1. Therefore, the G_R is equivalent to 33.8 dB. As a result, according to (5.4), $10\log_{10}(\frac{|\mathrm{B}(\mathbf{X},\theta,\phi)|^2}{\sigma^2(\theta)})$ should larger than 14.3359 dB. Therefore, the lower bound of mainlobe α can be calculated according to (3.34)

$$\alpha = 10^{(\frac{15.107}{20})} = 5.6931 \tag{5.5}$$

5.2 Simulation results

In this section, the simulation results for scenario 1 are shown in subsection 5.2.1 by changing the service angle θ_{svc} and minimum sidelobe angle θ_s. In subsection 5.2.2, the simulation results for scenario 2 are shown. We generate different beampatterns based on different sensor numbers.

5.2.1 Simulation results for scenario 1

By solving problem 3.44 through algorithm 1, the simulation results of LEO SAT beampattern synthesis which aims to achieve broadened mainbeam under CMC is shown. In the following simulations, we select the number of antenna elements as 32×32 and consider different SAT service beamwidth $2\theta_{\text{svc}} = 10°/20°/30°$. Besides, to avoid the sidelobe of URA beampattern overlapped with its mainlobe, we let the width of the transition region of ULA beampattern equals to $5°$, i.e., $|\theta_s^* - \theta_{\text{svc}}| = 5°$, where $\theta_s^* = \sin^{-1}(\frac{\sin(\theta_s)}{\sqrt{2}})$ is the minimum angle of the sidelobe of ULA beampattern and θ_s is the minimum angle of the sidelobe of URA beampattern, which can be derived from (4.5).

doi:10.6342/NTU202303344

5.2.1.1 SAT service beamwidth: $2\theta_{\text{svc}} = 10°$

sensor number	θ_{svc}	θ_s^*	θ_s	service area SNR_{min}	out-of-beam SNR_{max}
32×32	$5°$	$10°$	$14.22°$	5.1009 dB	-8.4492 dB

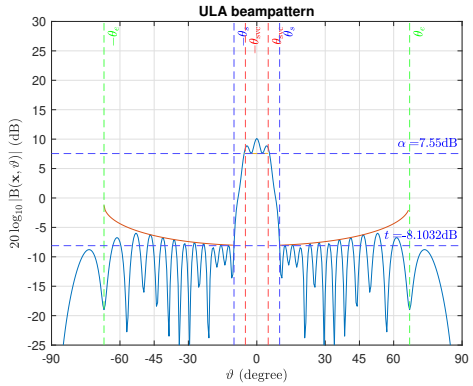

(a) ULA beampattern

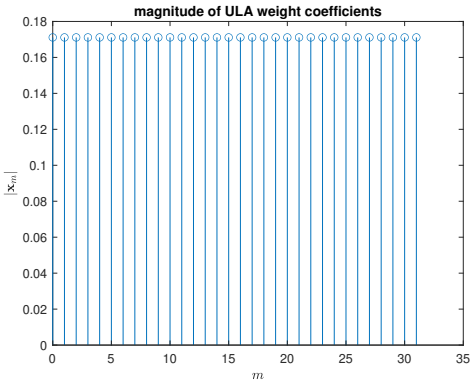

(b) ULA weight magnitude

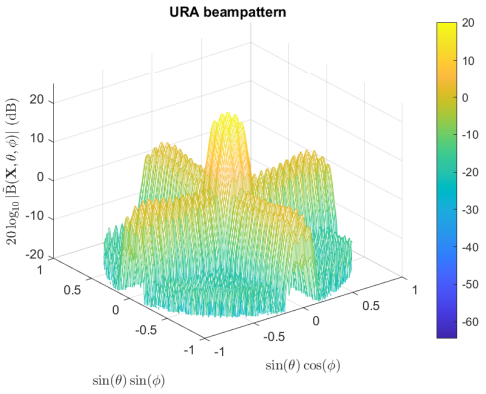

(c) URA beampattern

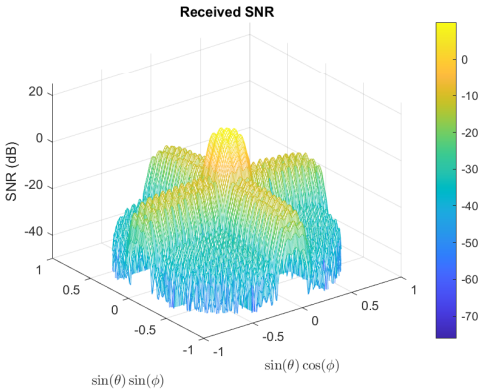

(d) Received SNR

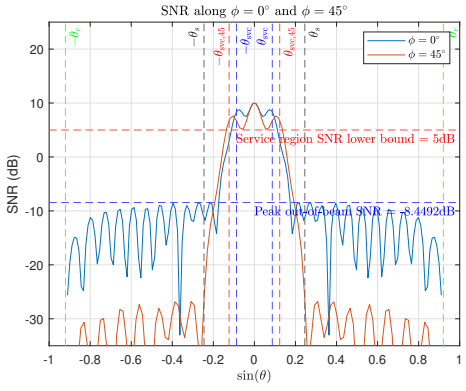

(e) Received SNR along $\sin(\theta)\cos(\phi)$ axis

doi:10.6342/NTU202303344

5.2.1.2 SAT service beamwidth: $2\theta_{\text{svc}} = 20°$

sensor number	θ_{svc}	θ_s^*	θ_s	**service area** SNR_{min}	**out-of-beam** SNR_{max}
32×32	$10°$	$15°$	$21.47°$	5.1348 dB	-3.2326 dB

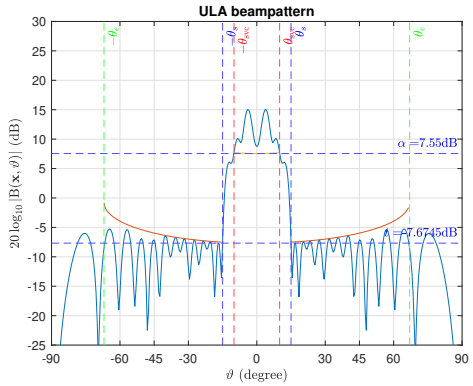

(a) ULA beampattern

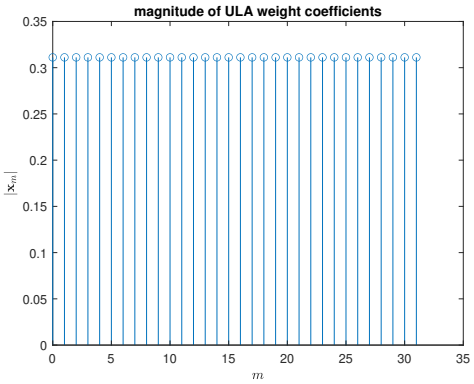

(b) ULA weight magnitude

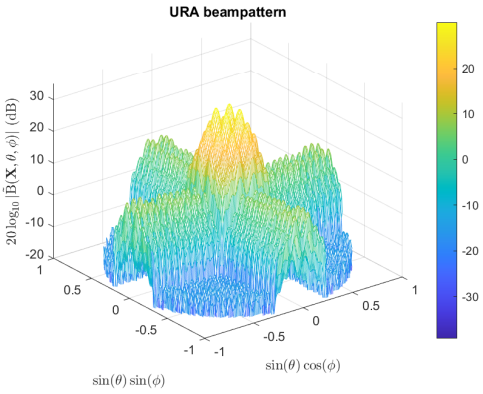

(c) URA beampattern

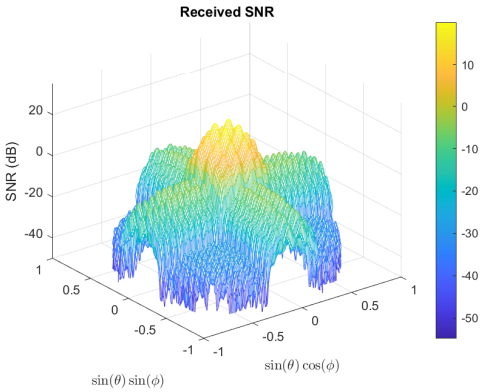

(d) Received SNR

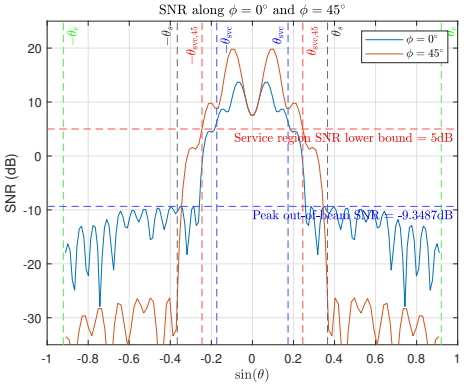

(e) Received SNR along $\sin(\theta)\cos(\phi)$ axis

doi:10.6342/NTU202303344

5.2.1.3 SAT service beamwidth: $2\theta_{\text{svc}} = 30°$

sensor number	θ_{svc}	θ_s^*	θ_s	**service area** SNR_{min}	**out-of-beam** SNR_{max}
32×32	15°	20°	28.93°	5.0158 dB	-9.6165 dB

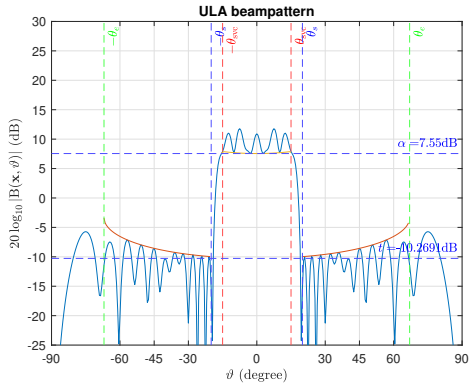

(a) ULA beampattern

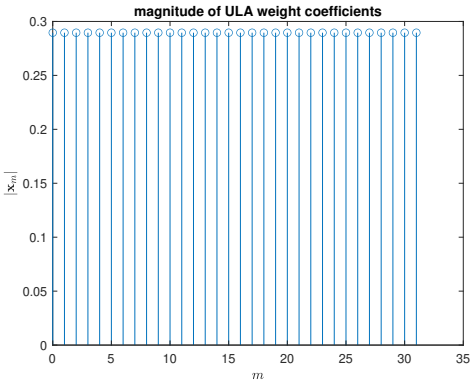

(b) ULA weight magnitude

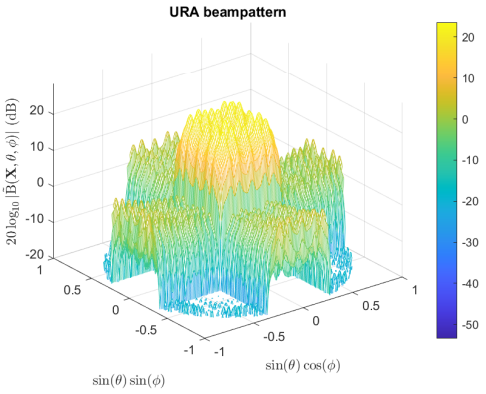

(c) URA beampattern

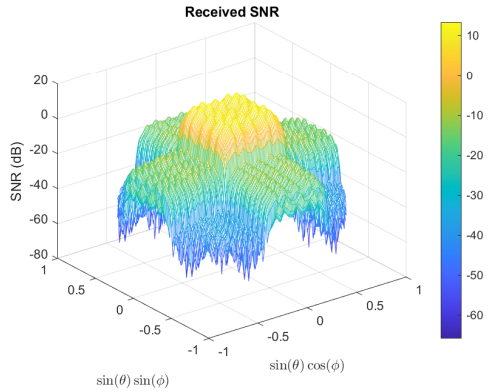

(d) Received SNR

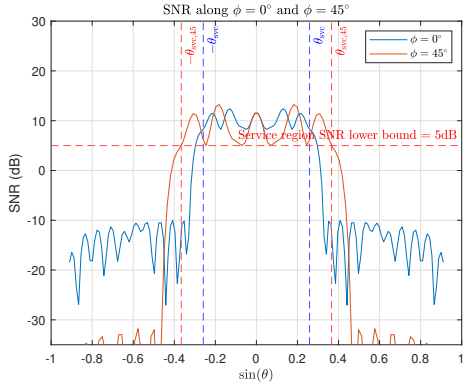

(e) Received SNR along $\sin(\theta)\cos(\phi)$ axis

doi:10.6342/NTU202303344

5.2.1.4 Remarks about simulation results of scenario 1

In table 5.2, minimum SNR in SAT service areas and maximum SNR in out-of-beam SAT service areas under the required SAT service beamwidth $2\theta_{\text{svc}} = 10°, 20°, 30°$ is shown.

Along $\sin(\theta)\cos(\phi)$ / $\sin(\theta)\sin(\phi)$ axis	$2\theta_{\text{svc}} = 10°$	$2\theta_{\text{svc}} = 20°$	$2\theta_{\text{svc}} = 30°$
Minimum SNR in SAT service areas	7.5189 dB	6.3542 dB	8.2605 dB
Maximum SNR in out-of-beam SAT service areas	-8.4492 dB	-9.3487 dB	-10.6212 dB
All illuminated areas	$2\theta_{\text{svc}} = 10°$	$2\theta_{\text{svc}} = 20°$	$2\theta_{\text{svc}} = 30°$
Minimum SNR in SAT service areas	5.1009 dB	5.1348 dB	5.0158 dB
Maximum SNR in out-of-beam SAT service areas	-8.4492 dB	-3.2326 dB	-9.6165

Table 5.2: SNR within and out of SAT service areas

From the simulation results and according to table 5.2, we can see that the minimum received SNR in service area is larger than 5dB no matter SAT service beamwidth $2\theta_{\text{svc}} = 10°/20°/30°$ which meets the constraint set in (3.43b). Besides, the beamforming weight coefficients meet CMC constraint in these cases which can ensure PA efficiency in practical application.

According to Table 5.2, we can achieve the received SNR gap of about 15.9dB, 15.7dB and 18.8dB when beamwidth is $10°$, $20°$ and $30°$ respectively along the $\sin(\theta)\cos(\phi)$ axis, where SNR gap is defined as the difference between the peak received SNR in out-of-beam area and the minimum SNR obtained in service area. While, in the mainlobe regions of the URA beampattern composited by the designed ULAs, we can only achieve received SNR gap of about 13.5dB, 8.3dB and 14.6dB when beamwidth is $10°$, $20°$ and $30°$ respectively. Also, we can observe that maximum SNR in out-of-beam SAT service

doi:10.6342/NTU202303344

areas is -9.3487 dB along $\sin(\theta)\cos(\phi)$ axis when $2\theta_{\text{svc}} = 20°$; while, it is -3.2326 dB within all illuminated areas.

The reason why maximum SNR at out-of-beam SAT service areas in all illuminated areas cannot be as low as the maximum SNR along $\sin(\theta)\cos(\phi)$ axis is that we cannot ensure obtaining URA beampattern with minimum PSL when decomposing URA beampattern design problem into two ULA beampattern design problems. Since the complexity is too high for us to directly solve the URA beampattern design problem with an array size of 32×32, so we take this approach. However, the tradeoff of this approach appears. The approach to achieve minimal PSL of URA beampattern by directly solving the URA design problem which can overcome the complexity will be our future work.

doi:10.6342/NTU202303344

5.2.2 Simulation results for scenario 2

By solving problem 3.46, we show the earth coverage beampattern synthesis with different number of antenna elements under CMC. SAT service angle θ_{svc} is set as SAT FoV angle θ_e obtained in (5.2). We will show the simulation results with URA antenna size $10\times10, 16\times16, 32\times32$, including the ULA beampattern, URA beampattern, beamforming weight coefficients, and the received SNR of UE in SAT beam areas.

5.2.2.1 URA antenna size 10×10

sensor number	θ_{svc}	service area SNR_{min}	Total weight power
10×10	67°	5 dB	2490

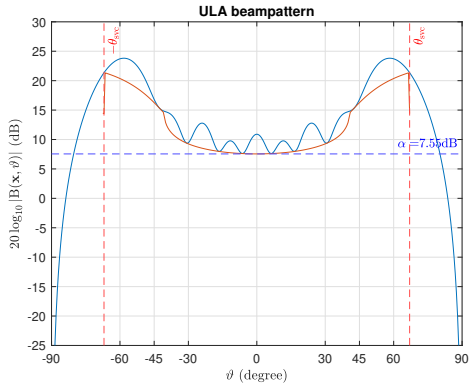

(a) ULA beampattern

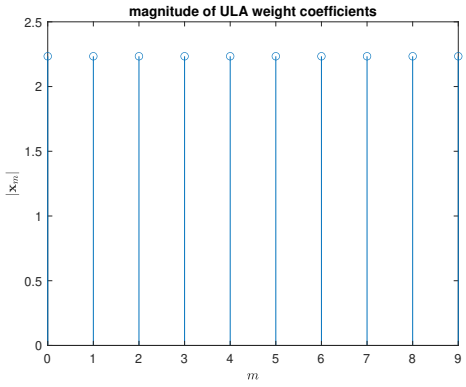

(b) ULA Weight magnitude

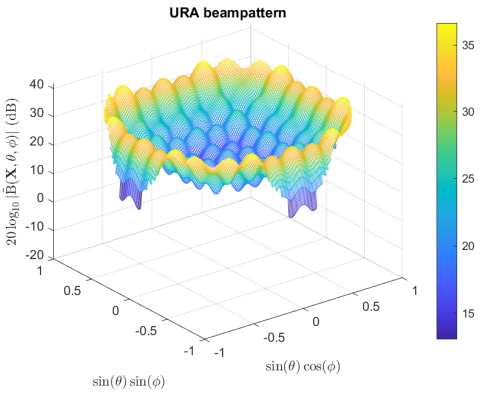

(c) URA beampattern

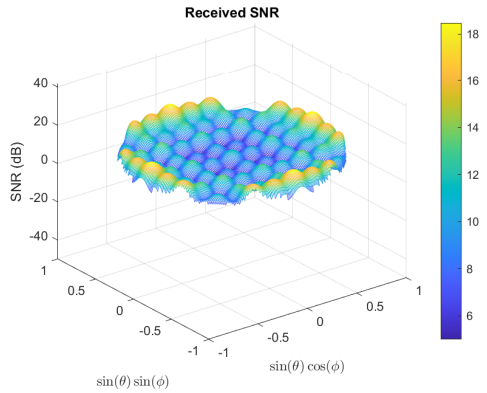

(d) Received SNR

doi:10.6342/NTU202303344

5.2.2.2 URA antenna size 16×16

sensor number	θ_{svc}	service area SNR_{min}	Total weight power
16×16	67°	5.0015 dB	1836

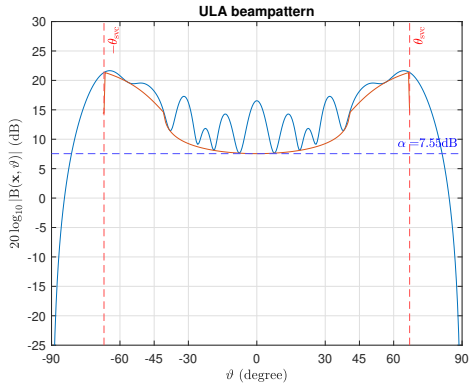

(a) ULA beampattern

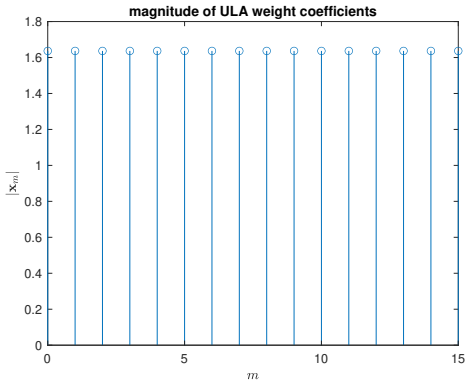

(b) ULA Weight magnitude

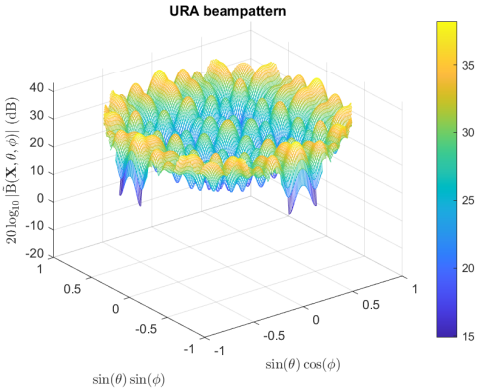

(c) URA beampattern

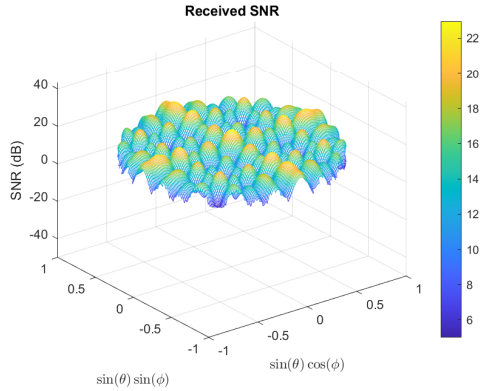

(d) Received SNR

doi:10.6342/NTU202303344

5.2.2.3 URA antenna size 32×32

sensor number	θ_{svc}	service area SNR_{min}	Total weight power
32×32	67°	5 dB	1278.5

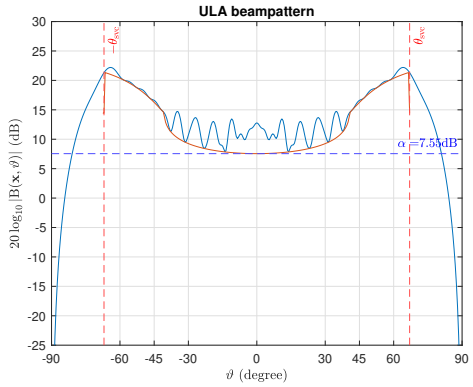

(a) ULA beampattern

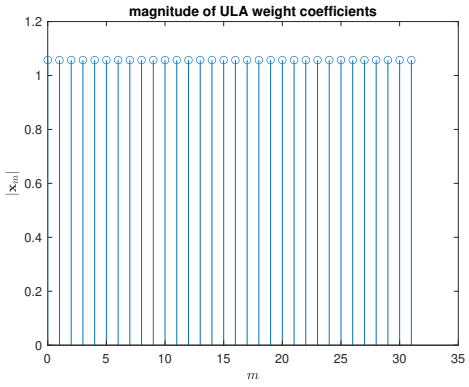

(b) ULA Weight magnitude

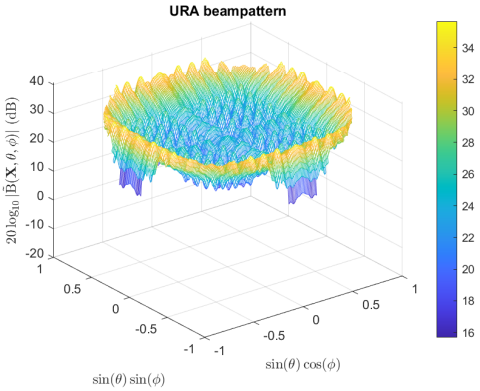

(c) URA beampattern

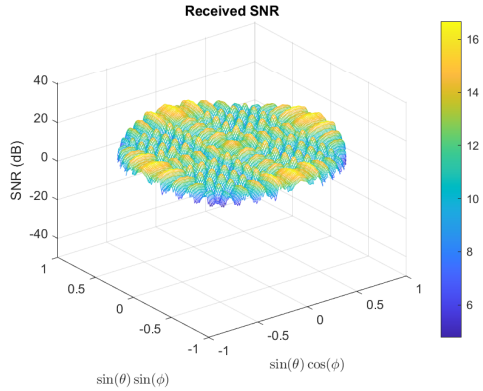

(d) Received SNR

doi:10.6342/NTU202303344

5.2.2.4 Remarks about simulation results of scenario 2

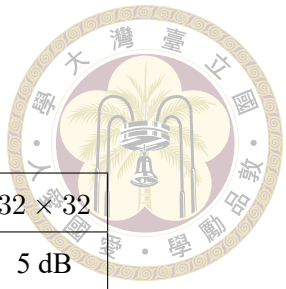

All illuminated areas	10×10	16×16	32×32
Minimum SNR in SAT service areas	5 dB	5.0015 dB	5 dB
Total weight power	2490	1836	1278.5

Table 5.3: SNR in SAT service areas and total weight power comparison

No matter the URA antenna size is 10×10, 16×16 or 32×32, the proposed ULA mask in 4.40 enables us to ensure the received SNR larger than 5dB in the mainlobe region which covers the Earth in the line of sight of a SAT. Besides, the beamforming weight coefficients that meet CMC can be achieved in all of the cases.

We observe that as the number of sensors becomes larger, we can obtain beamforming coefficients with less $\sum_{m=0}^{M_x-1}\sum_{n=0}^{M_y-1}|[\mathbf{X}]_{m,n}|^2$. Since the degree of freedom (DoF) of beamforming coefficients increases with a larger number of sensors, we are able to reduce the $\sum_{m=0}^{M_x-1}\sum_{n=0}^{M_y-1}|[\mathbf{X}]_{m,n}|^2$ power as more sensors are deployed. Since the total transmitted power is proportional to $\sum_{m=0}^{M_x-1}\sum_{n=0}^{M_y-1}|[\mathbf{X}]_{m,n}|^2$, as the number of sensors increase, we are able to save the energy used in SATCOM but also ensure the received SNR high enough for SAT service regions.

5.2.3 Comparison with previous works

We compare the proposed ULA beampattern to the beampattern in [Zhang2021][26] with the controllable mainbeam beamwidth and the CMC constraint. This paper aimed to suppress the peak sidelobe level without considering isoflux mask. Therefore, the upper bound of the ULA beampattern sidelobe was limited by a flat mask.

doi:10.6342/NTU202303344

sensor number	θ_{svc}	θ_s^*	θ_s
32×32	$15°$	$20°$	$28.93°$

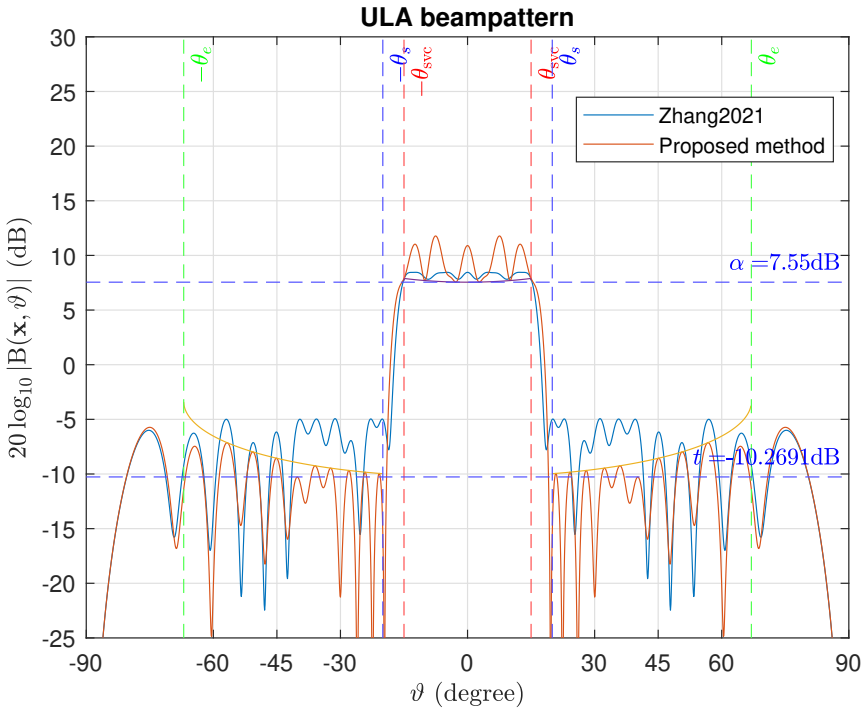

If we ensure the received SNR in service area is higher than 5dB in the both cases, the proposed method outperforms the previous work about 5dB for the suppression of peak received SNR in out-of-beam areas.

5.3 Channel capacity comparison

A larger average channel capacity can be achieved by applying wider beamwidth under the same total weight power. In this section, we first derive the beamwidth of steering vector array based on the 3GPP specification. Then, the signal-to-noise ratio comparisons between the proposed beampattern and that from steering vector array would be computed. Finally, we are able to compare the average channel capacity.

doi:10.6342/NTU202303344

5.3.1 Mainbeam beamwidth deduction for steering vector array

In 3GPP TR 38.821 [20], the normalized antenna gain corresponding to a typical reflector antenna with a circular aperture is formulated as following

$$|\tilde{\mathrm{B}}_N(\mathbf{X},\theta,\phi)|^2 = 4\left|\frac{J_1(ka\sin\theta)}{ka\sin\theta}\right|^2, \tag{5.6}$$

where $J_1(x)$ is the Bessel function of the first kind and first order with argument x, a is the radius of the antenna's circular aperture, $k = \frac{2\pi f}{c}$ is the wave number, f is the frequency of operation, c is the speed of light and θ is the angle measured from the bore sight of the antenna's main beam. Since the transmitted signal is narrowband, f can be replaced by carrier frequency f_c. Therefore, $k = \frac{2\pi}{\lambda_c}$, λ_c is the wavelength corresponding to f_c.

The relation between antenna gain and normalized antenna gain is

$$|\tilde{\mathrm{B}}(\mathbf{X},\theta,\phi)|^2 = P_{\text{peak}}|\tilde{\mathrm{B}}_N(\mathbf{X},\theta,\phi)|^2, \tag{5.7}$$

where P_{peak} is the peak power of the antenna gain.

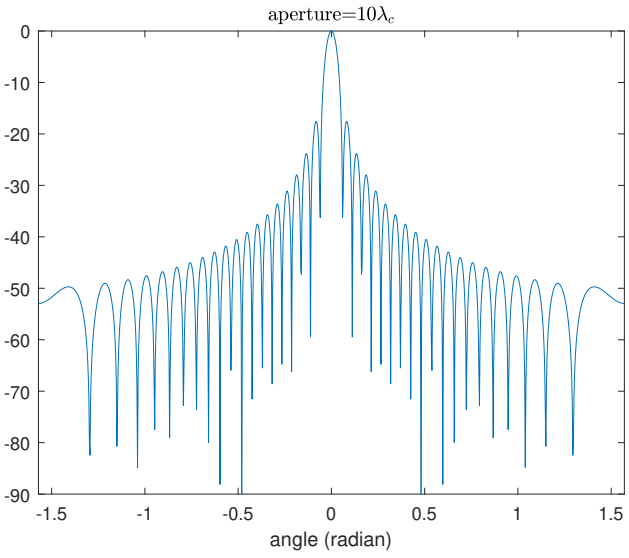

Figure 5.7: Example: 3GPP SatComm beampattern for aperture radius $10\lambda_c$

doi:10.6342/NTU202303344

This antenna gain is generated when the electric field strength at every point on continuous cylindrical polar coordinate of the antenna is constant [23]. However, a continuous cylindrical polar coordinate is impractical. Instead, we place N sensors on the antenna uniformly, then the electric field strength is decided by the excitations. In this way, every entry of $\mathbf{X}$ is constant to $\sqrt{\frac{P_{\text{tot}}}{N}}$, where P_{tot} represents total weight power $\sum_{i=0}^{N} |[\mathbf{X}]_i|^2$. Follow the assumption that every entry of $\mathbf{X}$ is $\sqrt{\frac{P_{\text{tot}}}{N}}$, the peak power of antenna gain P_{peak} equals to $P_{\text{tot}}N$.

Proof. The peak power of antenna gain P_{peak} is equivalent to $\max |\tilde{\text{B}}(\mathbf{X}, \theta, \phi)|^2$.

Recall (2.23),

$$\tilde{\text{B}}(\mathbf{X}, \theta, \phi) = \sum_{m=0}^{M_x-1} \sum_{n=0}^{M_y-1} [\mathbf{X}]^*_{m,n} e^{-j2\pi f_c(\frac{md_e \sin(\theta)\cos(\phi)+nd_e \sin(\theta)\sin(\phi)}{c})} \tag{5.8}$$

$$= \text{vec}(\mathbf{X})^H \tilde{\mathbf{a}}(\theta, \phi). \tag{5.9}$$

We define $\tilde{\mathbf{a}}(\theta, \phi) = \mathbf{a_m}(\theta, \phi) \otimes \mathbf{a_n}(\theta, \phi)$, where

$$\begin{aligned} \mathbf{a_m}(\theta, \phi) &= [1 \; e^{-j\pi f_c(\frac{d_e \sin(\theta)\cos(\phi)}{c})} \; ... \; e^{-j\pi f_c(\frac{(M_x-1)d_e \sin(\theta)\cos(\phi)}{c})}]^T, \\ \mathbf{a_n}(\theta, \phi) &= [1 \; e^{-j\pi f_c(\frac{d_e \sin(\theta)\sin(\phi)}{c})} \; ... \; e^{-j\pi f_c(\frac{(M_y-1)d_e \sin(\theta)\sin(\phi)}{c})}]^T \end{aligned} \tag{5.10}$$

Therefore, $\max |\tilde{\text{B}}(\mathbf{X}, \theta, \phi)|^2 = \max |\text{vec}(\mathbf{X})^H \tilde{\mathbf{a}}(\theta, \phi)|^2$. When every entry of $\mathbf{X}$ is $\sqrt{\frac{P_{\text{tot}}}{N}}$, the maximum value occurs at $(\theta, \phi) = (0, 0)$ since $\tilde{\mathbf{a}}(\theta, \phi)$ becomes a N-point

doi:10.6342/NTU202303344

vector whose entries are 1.

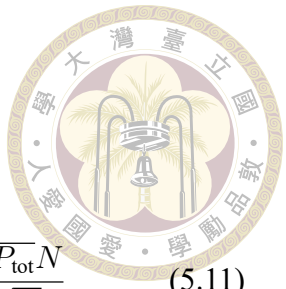

$$\tilde{\mathrm{B}}(\mathbf{X},\theta,\phi) = \begin{bmatrix} \sqrt{\frac{P_{\text{tot}}}{N}} & \sqrt{\frac{P_{\text{tot}}}{N}} & \cdots & \sqrt{\frac{P_{\text{tot}}}{N}} \end{bmatrix} \begin{bmatrix} 1 \\ 1 \\ \vdots \\ 1 \end{bmatrix} = \frac{\sqrt{P_{\text{tot}}N}}{\sqrt{N}} \tag{5.11}$$

$$\Rightarrow |\tilde{\mathrm{B}}(\mathbf{X},\theta,\phi)|^2 = P_{\text{tot}}N \tag{5.12}$$

□

Besides, to avoid spatial aliasing, the minimum element spacing should be $\frac{\lambda_c}{2}$. Therefore, the minimum value of a in (5.6) equals to $M_r \times \frac{\lambda_c}{2}$, where M_r is the number of sensors on the radius of the circular antenna. In this way, $k \times a = \frac{2\pi}{\lambda_c}\frac{M_r\lambda_c}{2} = M_r\pi$.

Assume there are 32×32 sensors on the circular antenna plate and suppose the sensors spread uniformly, the minimum required sensors on the plate radius is $M_r = \sqrt{\frac{1024}{\pi}} \approx 18$. To derive the 3-dB beamwidth,

$$0.5 = 4\left|\frac{J_1(M_r\pi\sin(\theta_{\text{svc}}))}{M_r\pi\sin(\theta_{\text{svc}})}\right|^2 \tag{5.13}$$

$$= 4\left|\frac{J_1(18\pi\sin(\theta_{\text{svc}}))}{18\pi\sin(\theta_{\text{svc}})}\right|^2 \tag{5.14}$$

$$\Rightarrow \theta_{\text{svc}} \approx 1.7189^\circ \tag{5.15}$$

We compare it to the proposed $\theta_{\text{svc}} = 5^\circ$ in scenario 1 (5.2.1.1). In this case, the total weight power $P_{\text{tot}} = \sum_{m=0}^{31}\sum_{n=0}^{31}|[\mathbf{X}]_{m,n}|^2 = 0.8779$.

$$P_{\text{peak}} = 1024 \times 0.8779 \tag{5.16}$$

doi:10.6342/NTU202303344

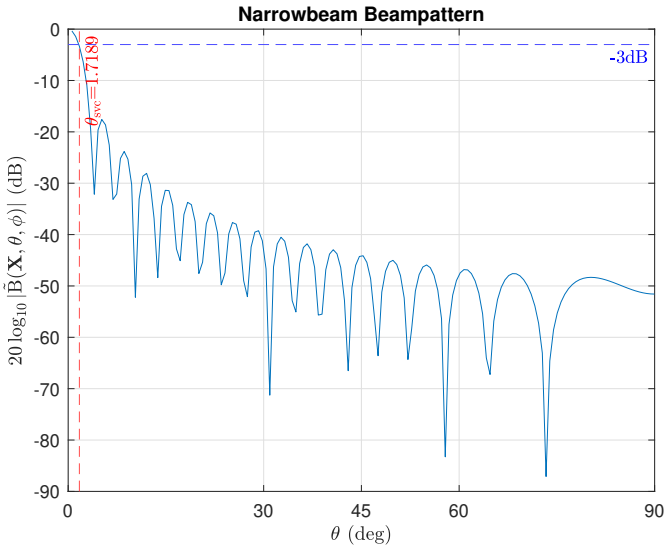

Figure 5.8: Narrowbeam beampattern

5.3.2 Signal-to-noise ratio comparison

According to (3.30), the signal-to-noise ratio (SNR) in the service region illuminated by the steering vector array is defined as

$$\mathrm{SNR}_{\mathrm{narrow}}(\mathbf{X}_n,\theta,\phi)=\frac{|\tilde{\mathrm{B}}(\mathbf{X}_n,\theta,\phi)|^2 G_R}{\sigma^2(\theta)kT_{\mathrm{sys}}f_{\mathrm{BW}}L_0} \tag{5.17}$$

On the other hand, the SNR of broadbeam is defined as

$$\mathrm{SNR}_{\mathrm{broad}}(\mathbf{X}_b,\theta,\phi)=\frac{|\tilde{\mathrm{B}}(\mathbf{X}_b,\theta,\phi)|^2 G_R}{\sigma^2(\theta)kT_{\mathrm{sys}}f_{\mathrm{BW}}L_0}, \tag{5.18}$$

where $\mathbf{X}_n$ is the excitation array of the narrowbeam beamformer and $\mathbf{X}_b$ is that of the proposed broadbeam beamformer.

The ratio of the SNR of narrowbeam to the SNR of broadbeam becomes

$$\frac{\mathrm{SNR}_{\mathrm{narrow}}(\mathbf{X}_n,\theta,\phi)}{\mathrm{SNR}_{\mathrm{broad}}(\mathbf{X}_b,\theta,\phi)}=\frac{|\tilde{\mathrm{B}}(\mathbf{X}_n,\theta,\phi)|^2}{|\tilde{\mathrm{B}}(\mathbf{X}_b,\theta,\phi)|^2} \tag{5.19}$$

doi:10.6342/NTU202303344

According to (5.12), $\max\{|\tilde{\mathrm{B}}(\mathbf{X}_n,\theta,\phi)|^2\} = P_{\text{tot}}N$. For the θ in 3dB-beamwidth, we ensure

$$|\tilde{\mathrm{B}}(\mathbf{X}_n,\theta,\phi)|^2 \geq (0.5P_{\text{peak}}) \tag{5.20}$$

The mainlobe lower bound for proposed beamformer has been derived in section 5.1.2.

$$|\tilde{\mathrm{B}}(\mathbf{X}_b,\theta,\phi)|^2 \geq \alpha^2\sigma^2(\theta), \tag{5.21}$$

where α is calculated according to (5.5). Therefore, we can derive

$$\text{SNR}_{\text{narrow}}(\mathbf{X}_n,\theta,\phi) \approx \text{SNR}_{\text{broad}}(\mathbf{X}_b,\theta,\phi) \times \frac{0.5P_{\text{peak}}}{\alpha^2\sigma^2(\theta)} \tag{5.22}$$

Since the service angle is small for narrowbeam beamformer, $\sigma(\theta) \to 1$

doi:10.6342/NTU202303344

5.3.3 Channel capacity comparison result

Let $C_{1,\text{avg}}$ be the average channel capacity of narrowbeam beamformers whose beams would be switched to achieve the total required coverage. Let C_2 be the channel capacity of the broadbeam beamformer. In the following demonstrations, we select the service beamwidth of the proposed beamformer to be 10° in scenario 1 (5.2.1.1).

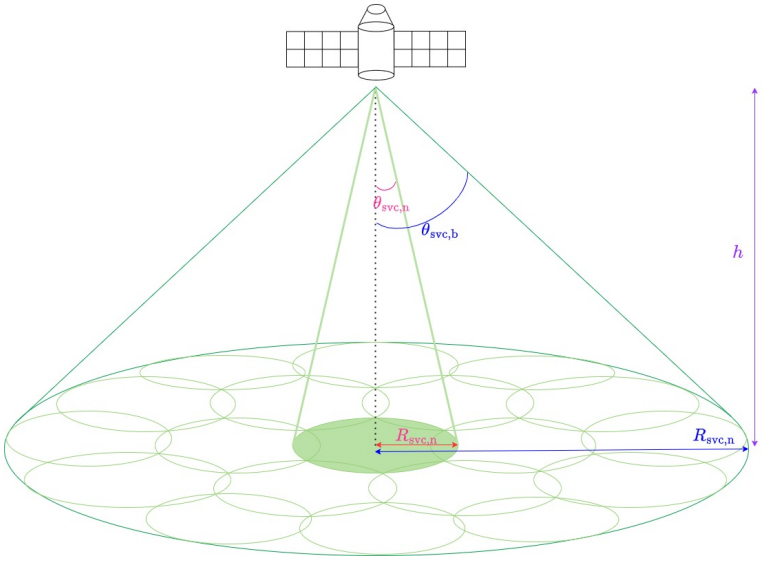

Figure 5.9: service region of broadbeam and narrowbeam

In figure 5.9, $\theta_{\text{svc,n}}$ denotes the service angle of narrowbeam beamformer and $\theta_{\text{svc,b}}$ denotes the service angle of proposed broadbeam beamformer. The service radius of narrowbeam beamfomer is denoted as $R_{\text{svc,n}} = h \cdot \tan(\theta_{\text{svc,n}})$ and that of broadbeam beamformer is denoted as $R_{\text{svc,b}} = h \cdot \tan(\theta_{\text{svc,b}})$. Follow (5.13), $\theta_{\text{svc,n}} = 1.7189^\circ$. We need $\frac{\tan^2(5)}{\tan^2(1.7189)} \approx 9$ beams to cover the service area of the proposed broadbeam beamformer.

doi:10.6342/NTU202303344

The average channel capacity of the narrowbeam beamformer is derived as

$$C_{1,\text{avg}} = \frac{1}{9} f_{\text{BW}} \log_2(1 + \text{SNR}_{\text{narrow}}) \tag{5.23}$$

$$= \frac{1}{9} f_{\text{BW}} \log_2(1 + \text{SNR}_{\text{broad}} \frac{0.5 P_{\text{peak}}}{\alpha^2}) \tag{5.24}$$

$$\downarrow P_{\text{peak}} = 899 \ (5.16), \quad \alpha = 5.6931 \ (5.5) \tag{5.25}$$

$$= \frac{1}{9} f_{\text{BW}} \log_2(1 + \text{SNR}_{\text{broad}} \frac{0.5 \times 899}{5.6931^2}) \tag{5.26}$$

The SNR larger than 5dB is desired (5.4), so we replace $\text{SNR}_{\text{broad}}$ with $10^{0.5}$. Consequently,

$$\frac{C_{1,\text{avg}}}{C_2} = \frac{1}{9} \frac{\log_2(1 + 10^{0.5} \times \frac{0.5 \times 899}{5.6931^2})}{\log_2(1 + 10^{0.5})} \tag{5.27}$$

$$= 0.2963 \tag{5.28}$$

As a result, the channel capacity of proposed broadbeam beamformer outperforms the average channel capacity of steering vector beamformer.

doi:10.6342/NTU202303344

doi:10.6342/NTU202303344

Chapter 6 Conclusion

6.1 Conclusion

In this thesis, two beam-broadening problems are formulated and solved. In scenario 1, we designed a transmit beamformer which enables the receivers in service area to obtain the SNRs higher than the required minimum SNR. Meanwhile, the received powers in SAT out-of-beam areas are suppressed. Also, to implement the amplifiers efficiently, CMC of beamforming coefficients is achieved. In scenario 2, we are able to achieve earth coverage beampattern synthesis and minimize the total SAT transmitted power to reduce the power consumption on a SAT. The simulation results demonstrate the obtained URA beampattern with broadened beamwidth which can ensure the received SNR in SAT service areas larger than minimum required SNR. The simulation results also show that the obtained beamforming coefficients meet CMC.

doi:10.6342/NTU202303344

6.2 Future work

In our work, URA beampattern synthesis problem is decomposed into two ULA beampattern synthesis problems due to the complexity issue. Through this approach, we cannot ensure to obtain URA beampattern with minimum PSL. If we can tackle the complexity issue of designing the URA beampattern synthesis problem when the array size is large, URA beampattern with a smaller PSL may be achieved.

doi:10.6342/NTU202303344

References

[1] Y. Albagory and F. Alraddady. Optimum extrapolation techniques for two-dimensional antenna array tapered beamforming. Electronics, 11(13), 2022.

[2] S. Chen, S. Sun, and S. Kang. System integration of terrestrial mobile communication and satellite communication —the trends, challenges and key technologies in b5g and 6g. China Communications, 17(12):156–171, 2020.

[3] I. Cohen, J. Benesty, and J. Chen. Differential kronecker product beamforming. IEEE/ACM Transactions on Audio, Speech, and Language Processing, 27(5):892–902, 2019.

[4] J. Dattorro. Convex Optimization and Euclidean Distance Geometry. Meboo Publishing, 2006.

[5] I. del Portillo, B. G. Cameron, and E. F. Crawley. A technical comparison of three low earth orbit satellite constellation systems to provide global broadband. Acta Astronautica, 159:123–135, 2019.

[6] M. Fazel, C. Fonteneau, M. Crussi‘ere, and B. Jahan. A systematic beam broadening method for large phased arrays. 2021 Joint European Conference on Networks and Communications & 6G Summit (EuCNC/6G Summit), pages 7–12, 2021.

doi:10.6342/NTU202303344

[7] A. Frank and I. Cohen. Constant-beamwidth kronecker product beamforming with nonuniform planar arrays. Frontiers in Signal Processing, 2, 2022.

[8] H. Friis and G. S.V.Kyriacou. A note on a simple transmission formula. Proceedings of the IRE, 34(5):254–256, May 1946.

[9] M. Grant and S. Boyd. CVX: Matlab software for disciplined convex programming, version 2.1. http://cvxr.com/cvx, Mar. 2014.

[10] A. Guidotti, A. Vanelli-Coralli, A. Mengali, and S. Cioni. Non-terrestrial networks: Link budget analysis. In ICC 2020 - 2020 IEEE International Conference on Communications (ICC), pages 1–7, 2020.

[11] M. Ibarra, M. A. Panduro, Ángel G. Andrade, and A. Reyna. Design of sparse concentric rings array for leo satellites. Journal of Electromagnetic Waves and Applications, 29(15):1983–2001, 2015.

[12] O. Kodheli, E. Lagunas, N. Maturo, S. K. Sharma, B. Shankar, J. F. M. Montoya, J. C. M. Duncan, D. Spano, S. Chatzinotas, S. Kisseleff, J. Querol, L. Lei, T. X. Vu, and G. Goussetis. Satellite communications in the new space era: A survey and future challenges. IEEE Communications Surveys & Tutorials, 23(1):70–109, 2021.

[13] S. Lei, W. Yang, Z. Lin, Z. He, H. Hu, Z. Zhao, and Y. Bao. An Excitation-DRR Control Approach for Wide-Beam Power Gain Pattern Synthesis. Signal Processing, 204:108858, 2023.

[14] A. Mahanfar. Uni-dimensional steering of phased array antennas. U.S. Patent 10 770 790 B1, September 2020.

doi:10.6342/NTU202303344

[15] A. Mahanfar. Uni-dimensional steering of phased array antennas, U.S. Patent 10, 770, 790 B1, Sep. 8, 2020.

[16] Z. quan Luo, W. kin Ma, A. M. cho So, Y. Ye, and S. Zhang. Semidefinite relaxation of quadratic optimization problems. IEEE Signal Processing Magazine, 27(3):20–34, May 2010.

[17] M. A. Richards. Fundamentals of Radar Signal Processing, 2nd ed. McGraw-Hill Education, 2014.

[18] W. Strickler, P. Correa, and G. Bollendorf. A better approach to measuring gan pa linearity. Microwave Journal, June 2020.

[19] Y. Su, Y. Liu, Y. Zhou, J. Yuan, H. Cao, and J. Shi. Broadband leo satellite communications: Architectures and key technologies. IEEE Wireless Communications, 26(2):55–61, 2019.

[20] G. T. . V15.4.0. Study on new radio (nr) to support non terrestrial networks (release 15). Technical report, Technical Specification Group Radio Access Network, September 2019.

[21] G. T. . v16.0.0. Solutions for nr to support non-terrestrial networks (ntn) (release 16). Technical report, Technical Specification Group Radio Access Network, December 2019.

[22] W. Wang, L. Gao, R. Ding, J. Lei, L. You, C. A. Chan, and X. Gao. Resource efficiency optimization for robust beamforming in multi-beam satellite communications. IEEE Transactions on Vehicular Technology, 70(7):6958–6968, 2021.

doi:10.6342/NTU202303344

[23] J. L. Whitrow. The radiation patterns of circular apertures. Technical report, National Security and ISR Division, Australia, May 2018.

[24] E. Yoshimoto and M. V. T. Heckler. Optimization of planar antenna arrays using the firefly algorithm. Journal of Microwaves, Optoelectronics and Electromagnetic Applications, 18(1):126–140, Jan 2019.

[25] C. Zhang, J. Yang, Y. Zhang, Z. Liu, and G. Zhang. Dynamic beam hopping time slots allocation based on genetic algorithm of satellite communication under time-varying rain attenuation. Electronics, 10(23), 2021.

[26] X. Zhang, X. Wang, and H. C. So. Linear arbitrary array pattern synthesis with shape constraints and excitation range control. IEEE Antennas and Wireless Propagation Letters, 20(6):1018–1022, 2021.

doi:10.6342/NTU202303344

Appendix A —

A.1 Objective function derivation for scenario 2

First, the transmitted power of URA toward a specific direction with elevation angle θ and azimuth angle ϕ is represented by $P_T \times G_T(\mathbf{X}, \theta, \phi)$, where P_T is defined in (3.4) and $G_T(\mathbf{X}, \theta, \phi)$ is defined in (3.6). Follow the assumption $\beta^2\mathbb{E}\{|s[k]|^2\} = 1$, $P_T \times G_T(\mathbf{X}, \theta, \phi) = |\tilde{\mathrm{B}}(\mathbf{X}, \theta, \phi)|^2$.

If we combine two ULA **x** and **y** into a URA **X** in the way of (4.2)

$$\mathbf{X} = \mathbf{x}\mathbf{y}^{\mathrm{T}} \text{ ,i.e, } [\mathbf{X}]_{m,n} = x_m y_n, m \in \mathbb{Z}_{M_x}, n \in \mathbb{Z}_{M_y}, \tag{A.1}$$

the relation between $\tilde{\mathrm{B}}(\mathbf{X}, \theta, \phi)$ and $\mathrm{B}(\mathbf{x}, \vartheta_x)$, $\mathrm{B}(\mathbf{x}, \vartheta_x)$ is shown as follows, which is explained detailedly in (4.3)

$$\tilde{\mathrm{B}}(\mathbf{X}, \theta, \phi) = \mathrm{B}(\mathbf{x}, \vartheta_x)\mathrm{B}(\mathbf{y}, \vartheta_y), \tag{A.2}$$

where $u = \sin(\theta)\cos(\phi) \in [-1, 1]$, $v = \sin(\theta)\sin(\phi) \in [-1, 1]$, $\vartheta_x = \sin^{-1}(u) \in [-\frac{\pi}{2}, \frac{\pi}{2}]$, and $\vartheta_y = \sin^{-1}(v) \in [-\frac{\pi}{2}, \frac{\pi}{2}]$.

Then, follow the definition of the mainlobe of composite URA beampattern in (4.3),

doi:10.6342/NTU202303344

the total transmitted signals of a SAT can be considered to be

$$\int_{-1}^{1}\int_{-1}^{1}|\mathrm{B}(\mathbf{x},\vartheta_x)\mathrm{B}(\mathbf{y},\vartheta_y)|^2 du dv \tag{A.3}$$

$$=\int_{-1}^{1}|\mathrm{B}(\mathbf{x},\vartheta_x)|^2 du \int_{-1}^{1}|\mathrm{B}(\mathbf{y},\vartheta_y)|^2 dv \tag{A.4}$$

$$=\frac{1}{\pi^2}\int_{-\pi}^{\pi}|\mathrm{B}(\mathbf{x},\vartheta_x)|^2 d\omega_x \int_{-\pi}^{\pi}|\mathrm{B}(\mathbf{y},\vartheta_y)|^2 d\omega_y, \tag{A.5}$$

where $\omega_x = \pi\sin(\vartheta_x)$ and $\omega_y = \pi\sin(\vartheta_y)$.

Theorem A.1.1 (Parseval's Theorem)**.** If $f(k) = \sum_{m=-\infty}^{\infty} c_m e^{jmk}$ and $f(k)$ is a periodic function of period 2π,

$$\frac{1}{2\pi}\int_{-\pi}^{\pi}|f(k)|^2 dk = \sum_{m=-\infty}^{\infty}|c_m|^2 \tag{A.6}$$

Recall the definition of ULA beampattern from (2.18),

$$\mathrm{B}(\mathbf{x},\vartheta_x) = \sum_{m=0}^{M-1} x_m^* e^{-jm\omega_x} \tag{A.7}$$

where $\omega_x = \pi\sin(\vartheta_x)$. Then, if we define x_m zero when $m \notin [0, M-1]$, we can see x_m^* as c_m and regard $\mathrm{B}(\mathbf{x},\omega_x)$ as $f(k)$. Therefore, applied with Parseval's theorem,

$$\frac{1}{2\pi}\int_{-\pi}^{\pi}|\mathrm{B}(\mathbf{x},\omega_x)|^2 d\omega = \sum_{m=-\infty}^{\infty}|x_m^*|^2 = \sum_{m=0}^{M-1}|x_m|^2. \tag{A.8}$$

We can bring (A.8) back into (A.5).

doi:10.6342/NTU202303344

$$\frac{1}{\pi^2}\int_{-\pi}^{\pi}|\mathrm{B}(\mathbf{x},\vartheta_x)|^2 d\omega_x \int_{-\pi}^{\pi}|\mathrm{B}(\mathbf{y},\vartheta_y)|^2 d\omega_y \tag{A.9}$$

$$=4\sum_{m=0}^{M-1}|x_m|^2\sum_{n=0}^{M-1}|x_n|^2 \tag{A.10}$$

$$=4\sum_{m=0}^{M-1}\sum_{n=0}^{M-1}|x_m|^2|x_n|^2 \tag{A.11}$$

$$=4\sum_{m=0}^{M-1}\sum_{n=0}^{M-1}|[\mathbf{X}]_{m,n}|^2 \tag{A.12}$$

As a result, the total weight power is proportional to the transmitted power of a SAT.

doi:10.6342/NTU202303344